Figure1.

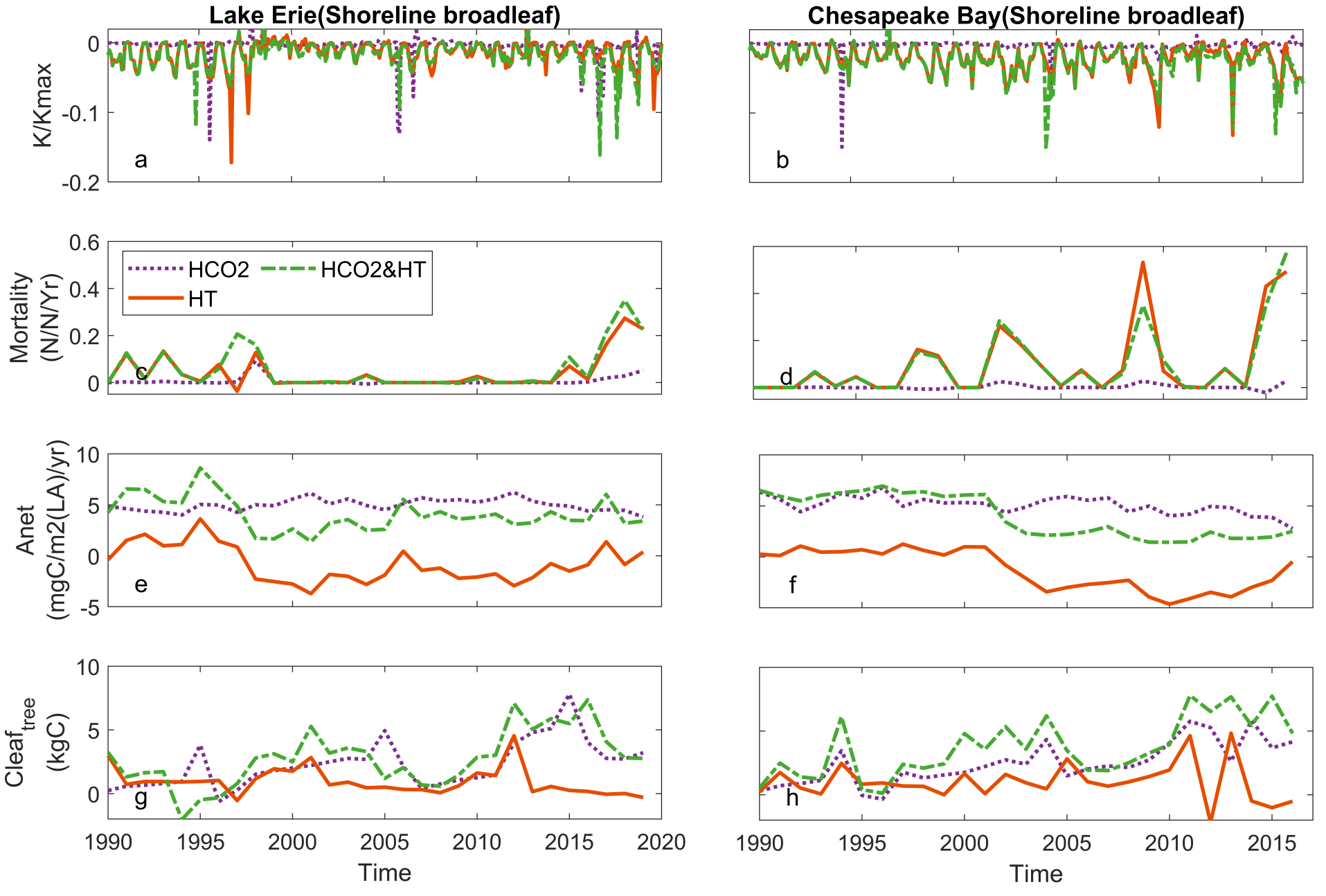
Lake Erie(Shoreline broadleaf)
Chesapeake Bay(Shoreline broadleaf)
K/Kmax
0
-0.1
-0.2
a
b
Mortality (N/N/Yr)
0.6
0.4
0.2
0
HCO2
HCO2&HT
HT
c
d
Anet (mgC/m2(LA)/yr)
10
5
0
-5
e
f
Cleaf tree (kgC)
10
5
0
g
h
1990
1995
2000
2005
2010
2015
2020
Time

Figure2.

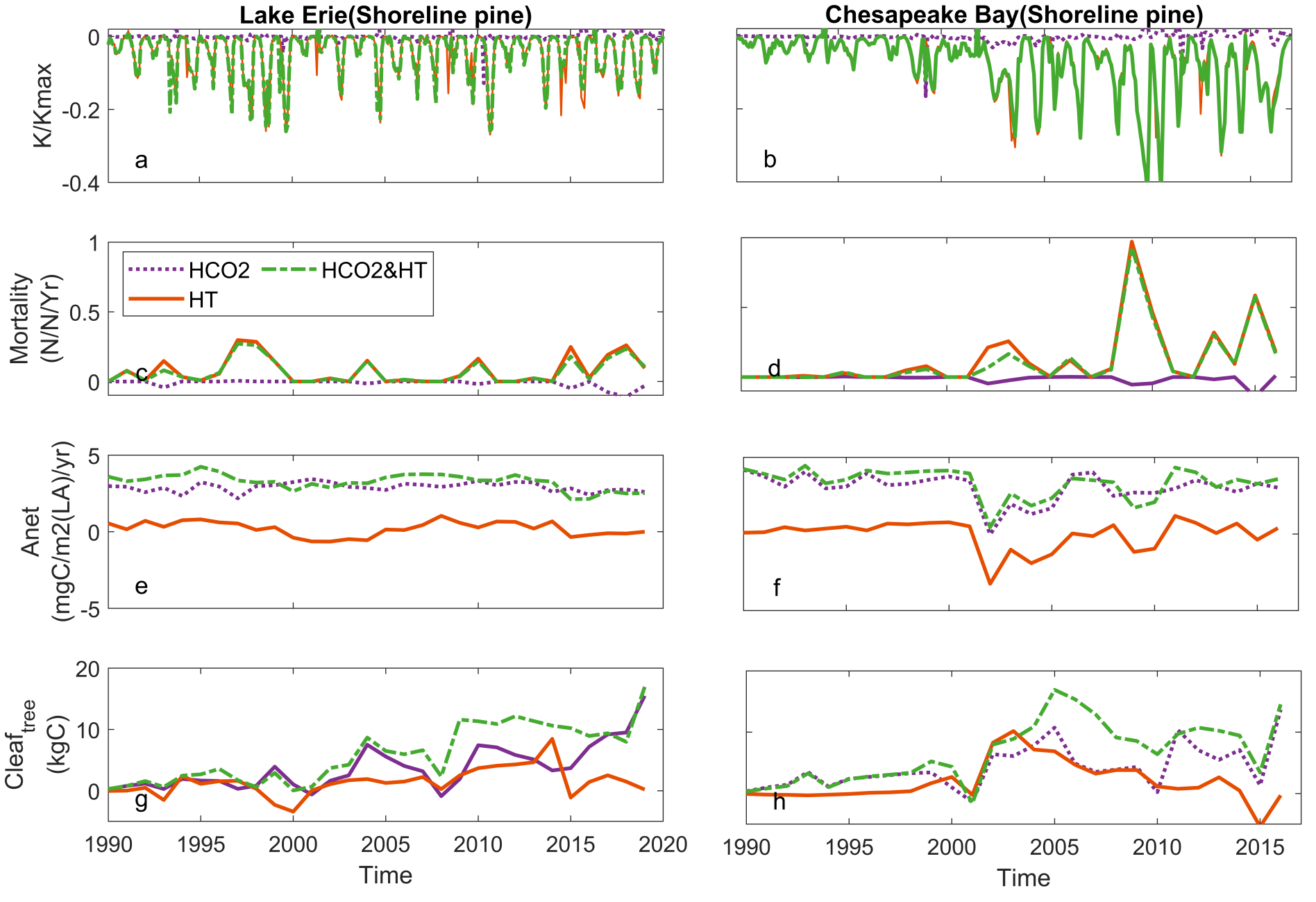
Lake Erie(Shoreline pine)
Chesapeake Bay(Shoreline pine)
K/Kmax
0
-0.2
-0.4
a
b
Mortality (N/N/Yr)
1
0.5
0
HCO2
HCO2&HT
HT
c
d
Anet (mgC/m2(LA)/yr)
5
0
-5
e
f
Cleaf tree (kgC)
20
10
0
g
h
1990
1995
2000
2005
2010
2015
2020
Time

Figure3.

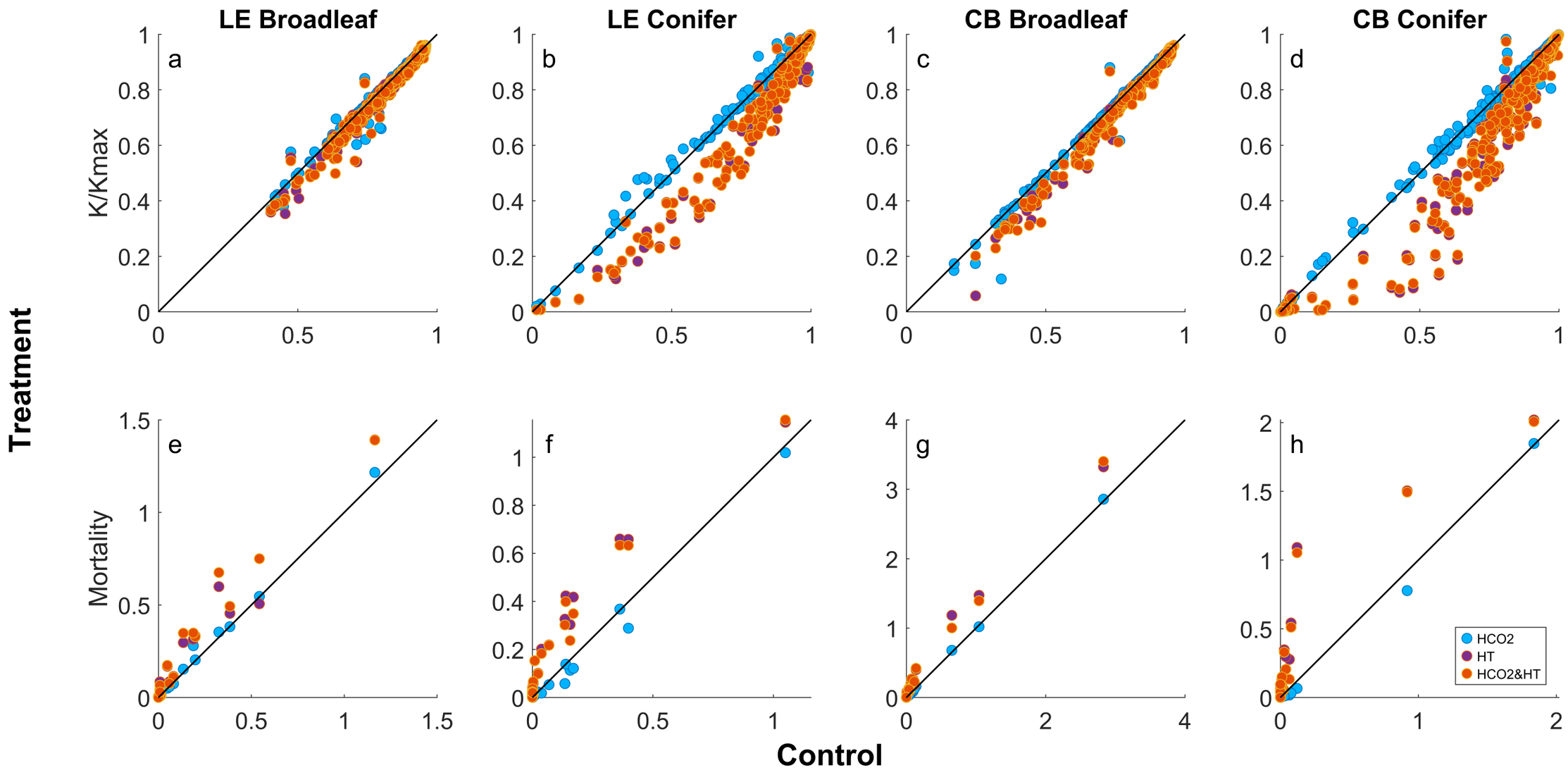
LE Broadleaf
LE Conifer
CB Broadleaf
CB Conifer
a
b
c
d
e
f
g
h
K/Kmax
Mortality
Treatment
Control
HCO2
HT
HCO2&HT

Figure4.

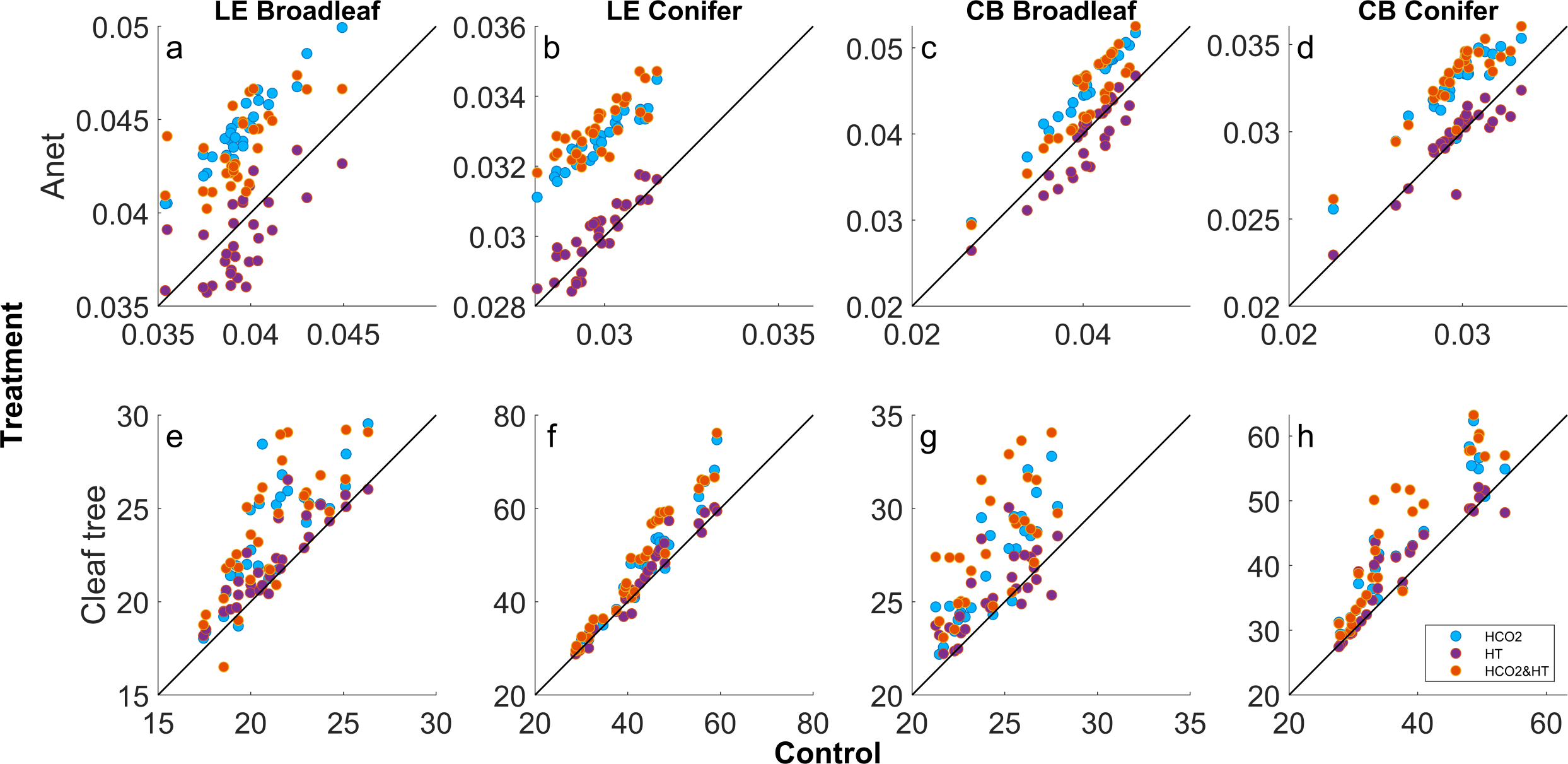
LE Broadleaf
LE Conifer
CB Broadleaf
CB Conifer
a
b
c
d
e
f
g
h
Anet
Cleaf tree
Treatment
Control
HCO2
HT
HCO2&HT

Figure5.

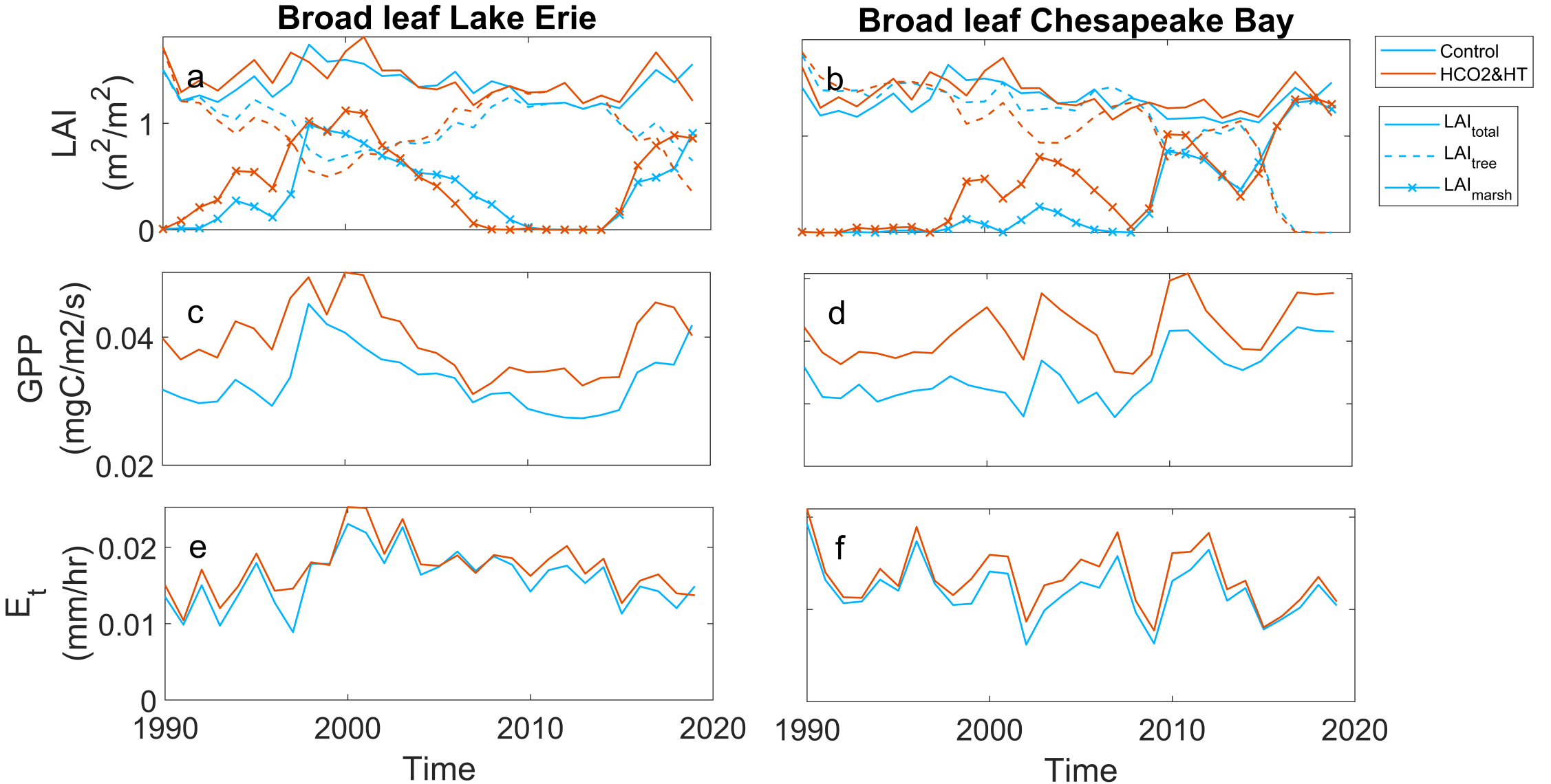
Broad leaf Lake Erie
Broad leaf Chesapeake Bay
a
b
c
d
e
f
LAI
(m2/m2)
GPP
(mgC/m2/s)
Et
(mm/hr)
0
1
0.02
0.04
0.01
0.02
1990
2000
2010
2020
Time
Control
HCO2&HT
LAItotal
LAItree
LAImarsh

Figure6.

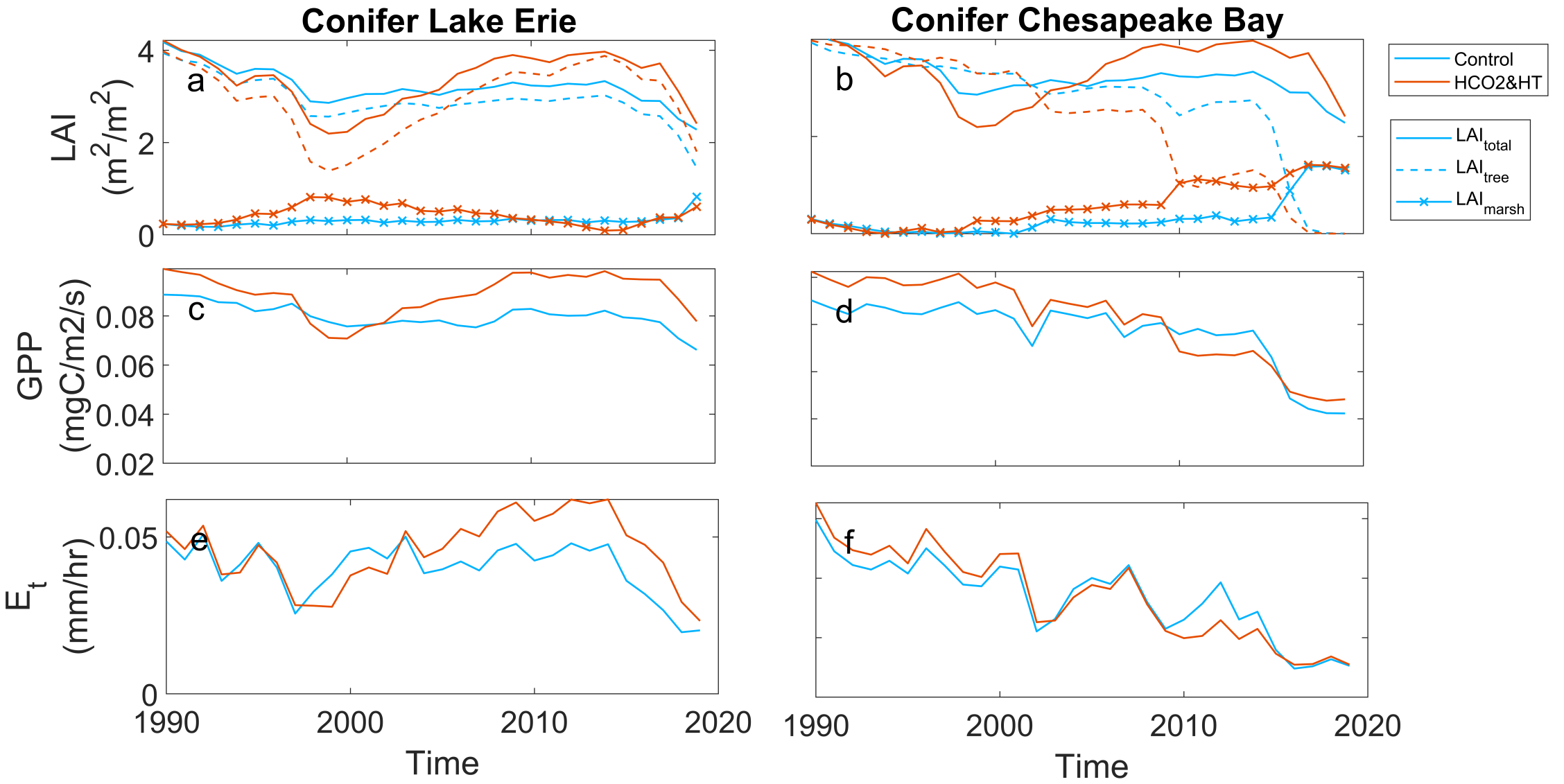
Conifer Lake Erie
Conifer Chesapeake Bay
a
b
c
d
e
f
LAI
(m2/m2)
GPP
(mgC/m2/s)
Et
(mm/hr)
0
2
4
0.02
0.04
0.06
0.08
0.05
1990
2000
2010
2020
Time
Control
HCO2&HT
LAItotal
LAItree
LAImarsh

Figure7.

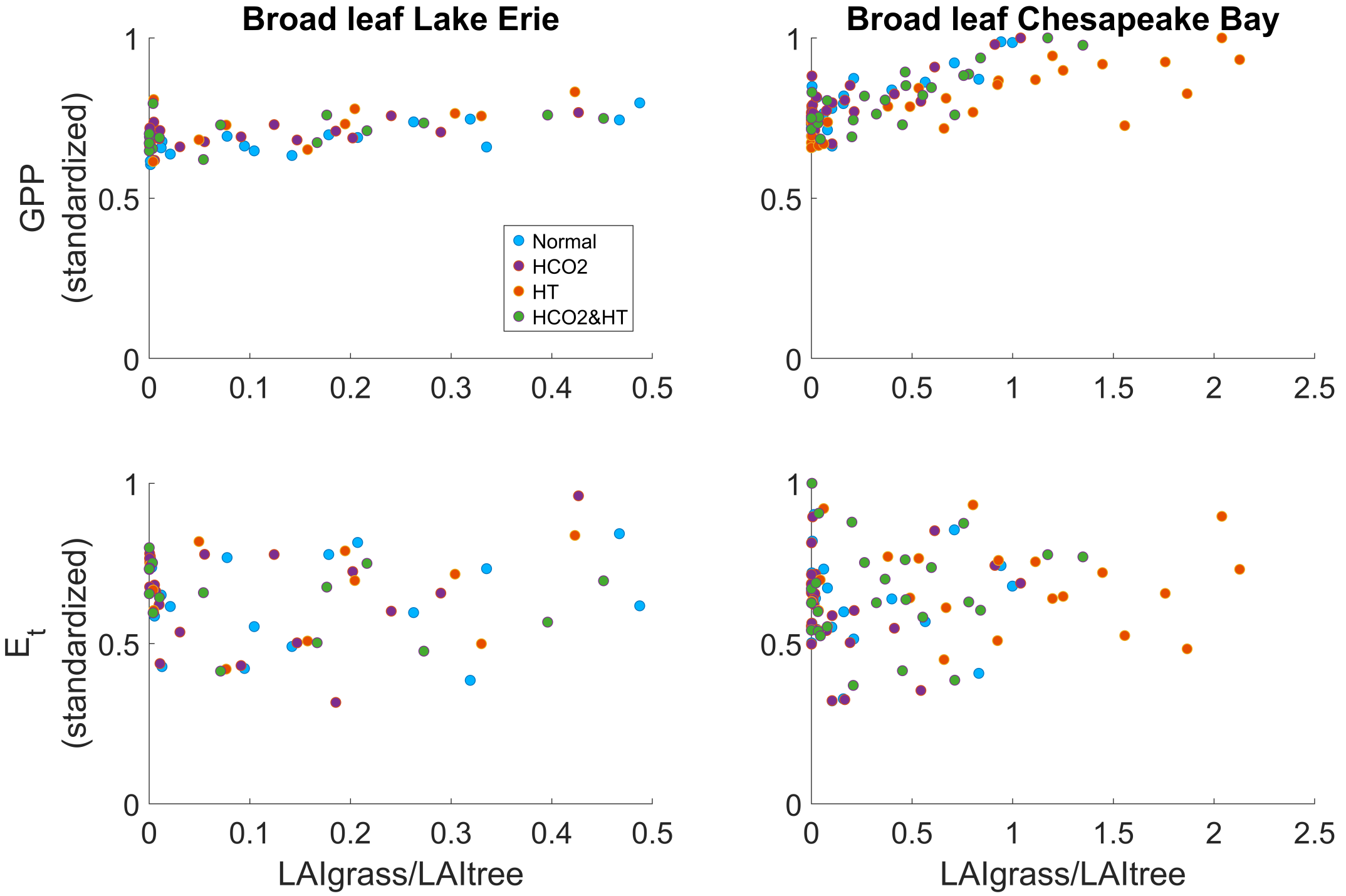
Broad leaf Lake Erie
Broad leaf Chesapeake Bay
GPP (standardized)
E_t (standardized)
LAIgrass/LAItree
LAIgrass/LAItree
Normal
HCO2
HT
HCO2&HT
0
0.1
0.2
0.3
0.4
0.5
0.5
1
1.5
2
2.5
1

Figure8.

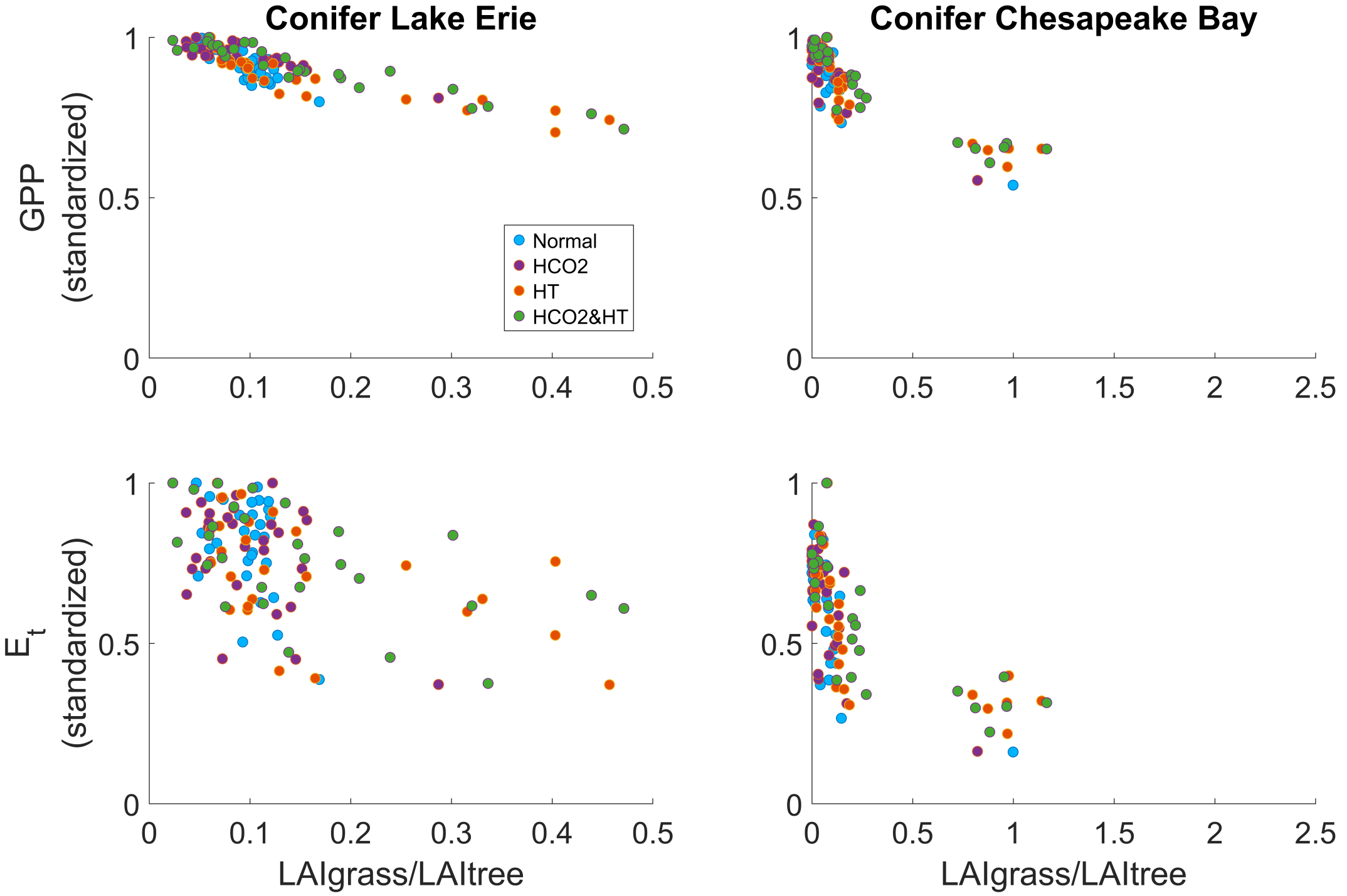
Conifer Lake Erie
Conifer Chesapeake Bay
GPP (standardized)
E_t (standardized)
LAIgrass/LAItree
LAIgrass/LAItree
Normal
HCO2
HT
HCO2&HT
0
0.5
1
0.1
0.2
0.3
0.4
1.5
2
2.5

Investigating coastal vegetation dynamics and ecosystem impacts under elevated CO_2 and temperature: A process-based approach

Junyan Ding[1] , Nate McDowell[2,3], Nate Conroy,[4] Donnie J. Day,[5] Yilin Fang,[6] Kenneth M. Kemner,[7] Matthew L. Kirwan,[8] Matthew Kovach,[5] Patrick Megonigal,[9] Kendalynn A. Morris,[10] Teri O'Meara,[11] Stephanie C. Pennington,[10] Roberta B. Peixoto,[5] Peter Thornton[11], Mike Weintraub,[5] Peter Regier,[12] Leticia Sandoval,[5] Fausto Machado-Silva,[5] Alice Stearns,[9] Nicholas D. Ward,[12] Stephanie J. Wilson[9] , Vanessa Bailey[2]

1. Department of Earth and Environment Science, Barcelona Supercomputing Center, Barcelona, Barcelona, Spain, 08034
2. Biological Science Division, Pacific Northwest National Laboratory, Richland, WA, USA, 99352
3. School of Biological Sciences, Washington State University, PO Box 644236, Pullman, WA, USA, 99164-4236
4. Earth and Environmental Sciences Division, Los Alamos National Laboratory, New Mexico, USA, 87545
5. Department of Environmental Sciences, The University of Toledo, Toledo, OH, USA, 43606
6. Earth Systems Science Division, Pacific Northwest National Laboratory, Richland, WA, USA, 99352
7. Biosciences Division, Argonne National Laboratory, Lemont, IL, USA 60439
8. Virginia Institute of Marine Science, College of William and Mary, Gloucester Point, VA, USA, 23062
9. Smithsonian Environmental Research Center, Edgewater, MD, USA, 21037
10. Joint Global Change Research Institute, Pacific Northwest National Laboratory, College Park, MD, USA, 20740
11. Environmental Sciences Division, Oak Ridge National Laboratory, Oak Ridge, TN, USA, 37830
12. Coastal Sciences Division, Pacific Northwest National Laboratory, Sequim, WA, USA, 98382

Corresponding author: Junyan Ding (jun.ding@bes.es; dingjunyan7@gmail.com)

Key points:

- In coastal forests, elevated temperature compounds hydraulic stress from salinity and submersion, increasing tree mortality beyond what would be expected in non-coastal forests.
- Elevated CO_2 enhances carbon uptake but does not reduce mortality arising from compound salinity and flooding stress.
- Broadleaf stands with more open canopies maintain productivity as marsh invades, whereas dense conifer stands lose productivity as marsh expansion lags behind tree mortality.

Abstract

Coastal forests are increasingly vulnerable to climate change and sea-level rise, with flooding and salinity driving transitions to marsh-dominated ecosystems. Using the coastal version of FATES-Hydro, we conducted 30-year simulations at two coastal forest sites—a broadleaf swamp white oak stand at Lake Erie and a conifer loblolly pine stand at Chesapeake Bay—under historical climate and elevated CO_2 (+100 ppm) and temperature (+1.5 °C) scenarios. Elevated CO_2 increased net primary productivity at both sites, while warming alone intensified hydraulic stress and accelerated mortality, particularly in the conifer stand. Simulations show that elevated temperatures intensify vapor pressure deficit and hydraulic stress on trees already experiencing salinity- and submersion-driven water stress, increasing tree mortality beyond what would be expected in a non-water-limited environment. Marsh expansion partially compensated for tree loss at the Lake Erie site but reduced ecosystem productivity in the conifer forest at Chesapeake Bay. Our results highlight how differences in stand structure, phenology, and local hydrology modulate ecosystem trajectories under climate change, emphasizing the importance of demographic and community-level processes for predicting the fate of coastal forests.

1. Introduction

Shoreline vegetation provides important ecosystem functions and services (Barbier et al., 2011; Mitsch et al., 2015), including high productivity in wetland compared to upland systems (Tagestad et al., 2021), larger carbon stocks in upland systems than the young marshes replacing them (Smith et al., 2021), reduced impacts of storms and erosion (Arkema et al., 2013; Spalding et al., 2014), and habitat for diverse animal species (Duarte et al., 2013; Barbier, 2013). Transitions from coastal forests to marshes through tree mortality driven by anomalous inundation from freshwater and saltwater have been observed globally (McDowell et al., 2022). Changes in vegetation composition can further alter ecosystem functions, including primary productivity and evapotranspiration (Kirwan & Megonigal, 2013; Gedan et al., 2009). With sea level rise and shifting precipitation regimes, flooding and inundation are expected to intensify

through 2100 (IPCC, 2021; Bamber et al., 2019), raising uncertainty about the persistence of existing forested coastlines.

Environmental variability alters key drivers that influence the rate and extent of forest-to-marsh transitions in coastal ecosystems. In particular, rising atmospheric CO_2 concentrations and associated increases in temperature and vapor pressure deficit (VPD) are expected to affect plant physiological responses and mortality risk (McDowell et al., 2022; Grossiord et al., 2020). Atmospheric CO_2 is projected to reach 600–800 ppm by the end of the century, and global temperatures are expected to rise 1.5 to 2.0°C above pre-industrial levels (IPCC, 2021; Meinshausen et al., 2020). These changes could enhance carbon fixation, respiration, and seasonal leaf area expansion, potentially increasing biomass growth and altering carbon allocation patterns (Walker et al., 2020; Way & Montgomery, 2015). In fact, such changes are already underway. However, plant responses to climate change depend not only on temperature and CO_2 but also on water and salinity stress—key constraints in coastal environments (Li et al., 2022).

Inundation-induced root loss has emerged as a primary driver of forest-to-marsh transitions in coastal systems, acting through its effects on hydraulic failure and tree mortality (Ding et al., 2025). Simulations conducted at freshwater lacustrine (Lake Erie) and brackish estuarine (Chesapeake Bay) shoreline sites suggested that salinity and hypoxia-induced root mortality significantly reduced canopy cover, enabling marsh expansion. The resulting declines in leaf area index (LAI) governed the trajectory and pace of marsh invasion, with conifer forests showing larger reductions in LAI, gross primary production (GPP), transpiration, and soil water uptake than broadleaf forests. These findings highlight how vegetation responses to environmental stress arise from the interplay of physiological mechanisms—such as root mortality, carbon assimilation, and hydraulic failure—rather than from any single trait. To predict future vegetation dynamics and ecosystem function under climate change, models must therefore represent these coupled, process-level interactions explicitly. This insight directly motivates the present study, which extends the Functionally Assembled Terrestrial Ecosystem Simulator with explicit plant hydraulics (FATES-Hydro) to explore how elevated CO_2 and temperature interact with flooding stress across forest types.

Understanding the extent to which physiological traits, demographic processes, and vegetation composition mediate coastal ecosystem responses to climate change remains a major challenge. While leaf-level processes like photosynthesis, stomatal conductance, and embolism vulnerability (P50) have been widely studied (Farquhar & von Caemmerer, 1982; Fisher et al., 2018; McDowell et al., 2022; Grossiord et al., 2020), these alone cannot capture the emergent ecosystem-level outcomes. Previous studies using the FATES-Hydro model highlighted the importance of vegetation composition and trait diversity in modulating responses to flooding and salinity (Ding et al., 2025), but the additional effects of elevated CO_2 and warming on these responses remain poorly understood.

In this study, we use the coastal version of a plant hydraulics-enabled vegetation demographic model, the Functionally Assembled Terrestrial Ecosystem Simulator (FATES-Hydro; Ding et al., 2023), which was recently enhanced to represent root mortality from inundation (Ding et al., 2025). We apply this model to investigate how aboveground traits and environmental drivers—including elevated temperature and CO_2—shape coastal tree mortality, marsh invasion, and associated changes in GPP. Numerical experiments were conducted at two shoreline sites: a freshwater system along Lake Erie shoreline, Ohio, and a saline coastal system along the Chesapeake Bay, Maryland. At each site, we virtually swapped a broadleaf and a conifer species across locations, simulating their responses to elevated CO_2, elevated temperature, and their combination. These simulations enable us to evaluate how ecosystem dynamics change in response to variations in species composition, inundation regime (freshwater vs. seawater), and future climate conditions.

At the individual tree level, we examine how elevated CO_2 and temperature interact with flooding stress to affect VPD, root loss, recovery, and species-specific mortality. At the ecosystem level, we assess how stand structure and function—including leaf area index (LAI), GPP, and transpiration—respond to changing environmental conditions across forest compositions. Together, these analyses aim to clarify the mechanisms by which hydrologic stress and climate change shape the future of coastal forests.

2. Methods

2.1 Study areas

At our two study sites, water stress arises from different combinations of flooding and salinity. At Lake Erie (LE), water stress primarily results from prolonged freshwater submersion and associated hypoxia during periods of high lake level. At Chesapeake Bay (CB), trees experience compound stress from waterlogging and soil salinity driven by seawater intrusion. These contrasts in baseline hydrologic and salinity regimes motivate our comparative numerical experiments.

The first site is a broadleaf deciduous forest ecosystem located on the south shore of Lake Erie (LE) in Ohio, USA (41.48°N, 83.06°W). The area experiences warm, humid summers and cold, snowy winters. The LE site is dominated by broadleaf deciduous forest, with *Carya laciniosa* and *Quercus bicolor* as the main angiosperm species. Lake Erie is one of the Great Lakes of North America—a system of interconnected freshwater lakes. Its water level varies on daily, seasonal, interannual, and decadal timescales due to complex interactions among climate, lake bathymetry, and upstream water levels (Burlakova et al., 2014). Increases in water level have led to widespread coastal tree mortality (Sippo et al., 2018).

The second site is a coastal conifer forest located in Chesapeake Bay (CB), Maryland, USA (38.5°N, 76.3°W) (Smith & Kirwan, 2021). The region also has warm, humid summers and cool winters. The Chesapeake Bay area is a hotspot for sea-level–driven coastal forest retreat, due to rapid relative sea-level rise (RSLR) across low-lying coastal plains (Schieder et al., 2018; Chen & Kirwan, 2022). The CB site is dominated by *Pinus taeda* forest and has experienced SLR rates of 6.84 mm yr^{-1} in recent decades (NOAA Sea Level Trends: https://tidesandcurrents.noaa.gov/sltrends/; STAR: https://www.star.nesdis.noaa.gov/socd/lsa/SeaLevelRise/), which were two to three times faster than the global average (Sallenger et al., 2012; Ezer & Corlett, 2012). This rapid rise has contributed to substantial tree mortality along low-elevation shorelines.

At the Lake Erie site, the shoreline water table often remains very close to or above the soil surface during spring and early summer, leading to prolonged periods of saturated soil and frequent exposure to hypoxic conditions (FigS1c). At the Chesapeake Bay site, empirical soil salinity estimates derived from tidal water level and surface-water salinity (following Ding et al., 2025) show pronounced seasonal and interannual variability (Fig S1e). Along the shoreline,

growing-season soil salinity frequently exceeds the salinity threshold (5PSU) used in the FATES-Hydro root-loss function, indicating the trees had already experienced substantial osmotic and ionic stress in the historical period. These baseline hydrologic and salinity regimes provide the background stress environment on which our elevated temperature and CO_2 scenarios are superimposed.

2.2 Model Configuration and Experimental Design

We conducted numerical experiments with two forest types—broadleaf deciduous and conifer—at shoreline locations along the Lake Erie and Chesapeake Bay coasts under historical and future elevated CO_2 and temperature conditions. We first describe the two modeled ecosystems (study areas), then outline the setup of the numerical experiments. We used a newly developed version of the ecosystem demography model, FATES-Hydro (Ding et al., 2023b, 2025), to conduct numerical experiments exploring how shoreline vegetation responds to elevated atmospheric CO_2 and temperature.

2.2.1 FATES-Hydro model description

The FATES is a vegetation demographic model that simulates physiological processes and competitive dynamics among cohorts of different plant functional types (PFTs) (Fisher et al., 2018; Koven et al., 2020), which has been coupled with the land surface model (ELM) component of the Energy Exascale Earth System Model (Golaz et al., 2020). The hydraulically enabled variant, FATES-Hydro, incorporates plant water transport processes and their interaction with carbon assimilation (Ding et al., 2023a). In this model, transpiration is determined by the product of total leaf area and unit leaf-area transpiration rate (J), which itself depends on stomatal conductance and the vapor pressure gradient between internal leaf spaces and the atmosphere.

The hydraulic module represents the root system, xylem, and leaves as interconnected porous media, with water flow regulated by tissue water potentials. These potentials are governed by plant-specific pressure–volume relationships and vulnerability to cavitation, following formulations by Manzoni et al. (2013) and Christoffersen et al. (2016). Stomatal behavior is based on the Ball–Berry model (Ball et al., 1984; Oleson et al., 2013; Fisher et al., 2015), with an

additional constraint imposed by leaf water potential via a water stress function, β_t, which scales with the ratio of current leaf water potential to the water potential at 50% stomatal closure (P50gs) (Christoffersen et al., 2016).

Soil moisture dynamics are resolved through multiple soil layers. Root distribution is allocated across layers using the two-parameter function from Zeng (2001). Water uptake from each layer is computed based on the water potential difference between the rhizosphere and absorbing roots, and on layer-specific root conductance, which depends on root biomass and traits such as specific root length. Further implementation details, sensitivity analyses, and model assumptions are documented in the technical documentation (FATES Development Team, 2021, https://fates-users-guide.readthedocs.io/projects/tech-doc/en/latest/index.html) and in recent literature (Koven et al., 2020; Xu et al., 2023; Ding et al., 2023a, 2023b; Robbins et al., 2024).

In this study, we use the coastal version of FATES-Hydro developed by Ding et al. (2023, 2025), which incorporates several physiological mechanisms representing the effects of salinity and hypoxia on coastal vegetation. In the coastal configuration used here, FATES-Hydro represents the impacts of seawater intrusion and flooding on trees through three coupled pathways: (i) osmotic effects on water availability, (ii) ionic effects on photosynthetic capacity and xylem vulnerability, and (iii) chronic damage to fine roots.

Daily soil salinity is translated into organ-level (root, stem, leaf) salinity using a root salt-exclusion function. Following Ding et al. (2023), we represent root salt tolerance with a root salt-exclusion trait, k_{ex}, that determines the fraction of soil salinity that is transmitted into organ salinity. A value of k_{ex} =0.8 corresponds to moderate salt exclusion (i.e. ~80% of salt at the root–soil interface is prevented from entering the xylem). In Ding et al. (2023), this value was chosen so that the combined salinity-driven reductions in photosynthetic capacity, increased xylem vulnerability, and loss of root conductance reproduced observed patterns of hydraulic damage, gas exchange, and crown dieback of Sitka spruce along the seawater exposure gradient at Beaver Creek, Washington (Zhang et al., 2021; Li et al., 2022). Because analogous, long-term salinity-manipulation datasets are not available for the broadleaf and loblolly pine forests considered here, we adopt the same moderately salt-sensitive k_{ex} value for both tree plant functional types as a first-order approximation and note this as a limitation of the current model configuration.

Salinity affects plant water relations and physiology through two distinct but interacting pathways that operate on different timescales. Osmotic stress arises primarily from salt dissolved in soil pore water, which lowers the osmotic potential of the soil solution and reduces the water potential gradient driving root water uptake—an effect sometimes described as chemical drought (Munns & Tester, 2008; Perri et al., 2017). This osmotic component operates on relatively fast timescales (hours to days) and limits water availability to the plant. In contrast, ionic stress results from the progressive accumulation of Na^+ and Cl^- ions within plant tissues, causing damage to cellular processes including photosynthetic machinery and membrane integrity; ionic stress develops more slowly (days to weeks) and can persist even after osmotic conditions ease (Munns & Tester, 2008; Perri et al., 2019). Salt tolerance encompasses a range of mechanisms beyond root-level salt exclusion, including osmoregulation, ion compartmentalization, and synthesis of compatible solutes (Munns & Tester, 2008). The current implementation in FATES-Hydro captures the primary osmotic and ionic pathways as described below, while acknowledging that additional salt-tolerance mechanisms are not yet represented.

Organ salinity is then converted into an osmotic potential term ($\Psi_{osm} = k_{osm} * Sal_{org}$) that is added to the matric and gravitational components of water potential, thereby reducing the water-potential gradient driving root water uptake. The organ salinity also represents ionic stress on leaf photosynthetic capacity and xylem vulnerability. Leaf photosynthetic capacity parameters (V_{cmax} and J_{max}) decline with increasing leaf salinity following a logistic response calibrated using gas-exchange measurements on Sitka spruce along a seawater-exposure gradient at Beaver Creek, Washington (Zhang et al., 2021; Ding et al., 2023). In FATES-Hydro, this empirical salinity– V_{cmax} relationship is intended to represent the component of photosynthetic decline associated with ionic damage to the photosynthetic apparatus—effects not captured by the osmotic pathway alone. However, we acknowledge that this empirical relationship is a lumped representation that cannot fully separate osmotic from ionic contributions to reduced photosynthetic capacity based on field observations alone. In practice, both pathways likely contribute to observed declines in Vcmax under salinity. The dual representation in FATES-Hydro (osmotic effects via water potential and ionic effects via the Vcmax relationship) is a modeling convenience that allows the two physiological pathways to be represented without double-counting, but should not be interpreted as implying that the two effects are empirically

distinguishable from gas-exchange measurements alone. The pressure-conductance curve of xylem shifts in proportion to xylem salinity, such that trees become more vulnerable to cavitation as internal salt concentrations increase (Ding et al., 2023).

Finally, cumulative exposure to saline and saturated soils reduces fine-root biomass and conductance via an empirical root-loss function driven by both the duration and intensity of saline/hypoxic conditions. This decline in root function is modeled using empirical stress-response relationships derived from observed patterns of crown dieback, mortality, and root biomass in seawater-exposed Sitka spruce at Beaver Creek (Zhang et al., 2021; Ding et al., 2023) and from field observations of root loss in coastal conifer stands (Ding et al., 2025). Key parameter values are listed in Table S1 of the Supporting Information; full equations are provided in Ding et al. (2023, 2025). These combined mechanisms allow the model to simulate vegetation responses to seawater intrusion, salinity-induced reductions in hydraulic function, and root mortality under current and future coastal conditions.

To provide context for these salinity- and hypoxia-response formulations, we note that this parameterization follows the coastal FATES-Hydro applications in Ding et al. (2023), where the salinity-response and root-loss functions (including k_{ex} = 0.8) were calibrated against long-term observations of Sitka spruce at the Beaver Creek seawater exposure gradient and then applied across multiple coastal conifer sites. In Ding et al. (2025), these same formulations were extended to broadleaf vegetation for simulations at the Chesapeake Bay site. Because comparable long-term salinity-manipulation datasets do not exist for swamp white oak or loblolly pine, we retain this moderately salt-sensitive parameter set as a first-order approximation and explicitly acknowledge this as a limitation of the current model configuration (see Section 4.6).

2.2.2 Numerical experiments

In our numerical experiments, each simulation included two plant functional types (PFTs): trees (either broadleaf or conifer) and grasses. We simulated both broadleaf–grass and conifer–grass combinations at both the LE and CB shoreline sites over 30 years (1990–2019). We adopted the same experimental setup as in Ding et al. (2025) by first simulating the LE site with its native

broadleaf trees and marsh vegetation, and the CB site with conifers and marsh. We then swapped tree types between sites—simulating broadleaf forests at CB and conifer forests at LE. Initialization data for pine at CB and oak at LE were used at both locations accordingly. Grass colonization originated from external seed supply in year one, followed by both external and local reproduction thereafter. Alongside meteorological inputs, daily soil salinity at CB and water table depth at LE were used as external driving variables (see Ding et al., 2023; 2025 for details).

At Lake Erie, the 'broadleaf deciduous tree' type represents the Quercus bicolor dominated stand, whereas at Chesapeake Bay the 'conifer tree' type represents the Pinus taeda dominated stand. Throughout the text we use 'broadleaf trees' and 'conifer trees' as shorthand for these species-dominated stands, rather than for generic plant functional types.

For all simulations we used a single set of salinity and hypoxia tolerance parameters for both broadleaf and conifer trees, including the root salt-exclusion coefficient, the salinity threshold for root loss, and the coefficients governing salinity-induced root mortality. These parameters were previously calibrated at the Beaver Creek coastal conifer site by matching simulated relationships between leaf and soil ion concentrations, crown dieback, and mortality to observations for Sitka spruce exposed to seawater flooding (Ding et al., 2023). Species-specific constraints on long-term salinity and flooding tolerance are not available for the Lake Erie and Chesapeake Bay forests; we therefore adopt this calibrated parameter set as a common, moderately salt-sensitive template for coastal trees in all simulations.

Trait parameters for the broadleaf and conifer trees were derived primarily from field measurements at the Lake Erie and Chesapeake Bay sites and complemented with values from published databases when observations were lacking. For both sites, $V_{cmax,25}$ and $J_{max,25}$ were estimated from A/Ci curves measured on the dominant species and then adjusted within the observed ranges so that simulated hourly net photosynthesis matched fitted relationships between net photosynthesis and intercellular CO_2. Hydraulic traits (maximum whole-plant conductance and the water potential at 50% stomatal closure) were calibrated within ranges observed for temperate broadleaf and conifer species so that simulated diurnal leaf water potentials reproduced observed patterns. Allometric parameters linking DBH to height, sapwood area,

woody biomass, and leaf biomass were derived from the BAAD database (Falster et al., 2015) and tuned so that simulated stand-level leaf area index matched site-level estimates. A complete list of parameters and their sources is provided in Table S1 and in the Supporting Information.

We ran simulations for 30 years under four climate scenarios: (1) historical climate, (2) elevated atmospheric CO_2, (3) elevated temperature, and (4) combined elevated CO_2 and temperature. These scenarios are denoted as Control, HCO2, HT, and HCO2&HT, respectively. The same plant parameter sets from Ding et al. (2025) were used throughout. In ELM, ambient vapor pressure is calculated from air temperature and relative humidity, so increasing temperature automatically increases vapor pressure deficit (VPD).

Meteorological forcing used to drive the model was derived from the University of East Anglia Climatic Research Unit Japanese Reanalysis (CRUJRA) dataset (Harris, 2019), spanning 1990–2019. Atmospheric CO_2 concentrations were set at 400 ppm for the historical scenario and 500 ppm for elevated CO_2 scenarios. In elevated temperature scenarios, air temperature was uniformly increased by 1.5°C above the corresponding historical CRUJRA values. Daily soil salinity and water table depth at CB, as well as water table depth at LE, were used as additional external drivers in the simulations. For LE, daily water table depth from 1990 to 2019 was reconstructed by establishing a linear relationship between shoreline water table measurements in 2022 and water level records from the NOAA station in Cleveland, which was then applied to the historical data (Ding et al., 2025). During the simulation, lake levels were notably high during two periods: 1997–1999 and 2018–2020 (FigS1b). At CB, soil salinity was derived from an empirical relationship between open water level and salinity (Ding et al., 2023b). Estimated soil salinity showed seasonal and interannual fluctuations, with a gradual increasing trend over the simulation period (FigS1e). This approach captures first-order variability in pore-water salinity but does not resolve fine-scale heterogeneity associated with microtopography, evapotranspiration, or species-specific salt-exclusion strategies; thus, the simulated salinity time series should be interpreted as a site-level approximation rather than a detailed prediction. We used the observed upland inventory data of Carya spp. at LE for both CB and LE initialization and observed upland inventory data of Pinus spp. at CB for both CB and LE initialization. The simulated marsh colonization was from external seed supply at the first year, then from both external seed supply and local reproduction afterward.

3. Results

3.1 Tree-level hydraulic and carbon responses to elevated CO_2 and temperature

We first examine how elevated temperature and CO_2 affect tree hydraulic function, mortality, and carbon assimilation under flooding, using simulations for both broadleaf and conifer trees across the two shoreline ecosystems. Simulations run with historical CO_2 and climate serve as the control. Treatment impacts are presented as the difference from the control (i.e., treatment minus control), where zero indicates no treatment effect, a positive value indicates an increase, and a negative value indicates a decrease.

Broadleaf trees exhibited increased xylem conductivity loss (up to 45% at CB and 35% at LE) and higher mortality (peaking at 12% yr^{-1} under elevated temperature at CB) under elevated temperature, reflecting the compounding effects of increased VPD during high water or salinity periods (Fig. 1a–d). In contrast, elevated CO_2 enhanced both net leaf carbon assimilation (A_{net}) (by ~25–35%) and total leaf biomass (by ~30%) (Fig. 1e–h). When both temperature and CO_2 were elevated, the positive effect of CO_2 on carbon gain partially offset the negative effects of temperature-induced stress on mortality.

Conifer trees exhibited a similar pattern: elevated temperature increased xylem conductivity loss (by ~50% at CB and ~40% at LE) and mortality (reaching 15% yr^{-1} under elevated temperature at CB) (Fig. 2a–d), while elevated CO_2 increased Anet (by ~20–30%) and leaf biomass (by ~25%) (Fig. 2e–h). However, the temperature effects on carbon budgets were generally weaker in conifers than in broadleaf trees.

Across species, elevated temperature induced greater xylem conductivity loss (up to 50%) and mortality (10–15% yr^{-1}) in conifers compared to broadleaf trees at both sites (Fig. 3a–d). Responses were consistent across sites for each species. Elevated CO_2 had similarly positive effects on Anet and leaf biomass in both groups, with stronger responses observed at Lake Erie than at Chesapeake Bay (Anet increased by ~30% at LE vs. ~20% at CB) (Fig. 4a–h). While

elevated temperature slightly reduced A_{net} of broadleaf trees (by ~5%; Fig. 4a, c), it had negligible effects on conifer A_{net} (Fig. 4b, d).

In the historical simulations, Chesapeake Bay shoreline trees experienced soil salinity above the root-loss threshold on a substantial fraction of growing-season days, whereas Lake Erie shoreline trees encountered saturated or near-saturated soils for a large portion of the spring and early summer. These baseline stress frequencies are summarized in Fig. S1 and highlight that both sites are already operating under strong hydrologic and salinity constraints before any climate perturbation is applied.

3.2 Ecosystem responses mediated by vegetation composition

At the ecosystem scale, vegetation composition strongly influenced forest responses to elevated CO_2 and temperature. These effects were most pronounced in LAI, GPP, and transpiration, following marsh expansion driven by climate-induced tree mortality.

In broadleaf forest ecosystems, treatments with elevated CO_2 and temperature accelerated tree mortality (cumulative tree cover decline of ~40% at CB and ~30% at LE) and marsh expansion (marsh area increased to ~60% of total cover at CB and ~50% at LE) relative to historical conditions (Fig. 5a–b). Despite these changes in vegetation composition, total LAI remained relatively stable (fluctuating within ±10% of control values) throughout the simulation. GPP was slightly higher under the treatments (increased by ~5–10%), and transpiration showed modest increases (by ~5%) (Fig. 5c–f). Broadleaf systems at Lake Erie exhibited quicker recovery after flooding than those at Chesapeake Bay.

In conifer forest ecosystems, elevated CO_2 and temperature also led to faster tree mortality (cumulative tree cover decline of ~50% at CB and ~40% at LE) and marsh expansion (marsh area increased to ~30–40% at CB but remained <20% at LE) (Fig. 6a–b). However, these systems exhibited greater variability in LAI and GPP, with pronounced declines during stress periods (LAI decreased by up to 50% and GPP dropped by ~30% at CB) and less consistent recovery (Fig. 6c–d). Transpiration also fluctuated more in conifer systems (by ±20%) than in broadleaf systems (by ±10%) (Fig. 6e–f). As with broadleaf systems, recovery at Lake Erie was more apparent than at Chesapeake Bay.

To assess whether the relationship between vegetation composition and ecosystem function remained consistent across scenarios, we analyzed how GPP and transpiration varied with the marsh-to-tree abundance ratio (Figs. 7 and 8). In broadleaf systems, GPP slightly increased with marsh expansion (by ~5–10%), while transpiration remained largely unchanged (within ±5%) (Fig. 7). In conifer systems, increases in marsh dominance corresponded to declines in both GPP (by ~20–25%) and transpiration (by ~15–20%) (Fig. 8). These trends were consistent across all climate scenarios. Soil water uptake remained similar across all treatments (data not shown).

4. Discussion

Our simulations with FATES-Hydro revealed several key findings. First, elevated temperature increased tree mortality in both broadleaf and conifer forests by intensifying hydraulic stress (Figs. 1a–d, 2a–d, 3a–d), with minimal impact on carbon assimilation (Figs. 1e–f, 2e–f, 4a–d). Second, elevated CO_2 consistently enhanced leaf-level carbon assimilation and biomass production (Figs. 1g–h, 2g–h, 4e–h), but did not alleviate water stress or reduce mortality at elevated temperature. Third, while tree-level physiological responses were broadly similar between conifers and broadleaf species, contrasting canopy structures and initial tree stand densities led to divergent ecosystem-scale outcomes. In particular, marsh invasion in broadleaf forests compensated for tree loss and maintained productivity (Fig. 5), whereas conifer forests—characterized by higher initial density and greater mortality—exhibited slower marsh expansion and greater declines in LAI and GPP (Fig. 6). Across all scenarios, stand composition—reflected in structure, density, and tree-to-marsh ratios—emerged as a stronger control on ecosystem carbon and water fluxes than physiology alone (Figs. 7–8).

The +1.5 °C and +100 ppm CO_2 perturbations we impose are modest relative to the magnitude of baseline hydrologic and salinity stresses at our sites. At the Chesapeake Bay shoreline, trees already experience high salinity for a substantial fraction of the growing season, and at Lake Erie, trees frequently experience saturated soils during spring. Our simulations should therefore be interpreted as showing how projected changes in temperature and CO_2 modify an already stressed system, rather than as responses to climate change in an otherwise benign environment.

4.1 Elevated temperature increases hydraulic stress without reducing carbon gain

Elevated temperature intensified hydraulic stress in both species by increasing VPD, which enhanced transpiration and exacerbated xylem conductivity loss and mortality (Figs. 1, 3). This is consistent with prior work showing that rising VPD is a key driver of hydraulic failure (Grossiord et al., 2020; Li et al., 2022). The mechanistic basis is captured by the relationship $\Delta\psi = J \times R_{root}$, where $\Delta\psi$ is the water potential drop from soil to stem, J is water flux, and R_{root} is root resistance, in which flooding and/or salinity-induced root loss increases while simultaneously elevated VPD increases J, compounding overall stress (Ding et al., 2025).

Despite increased hydraulic stress, A_{net} remained largely unchanged (Figs. 1e–f, 2e–f, 4a–d). This pattern does not imply that temperature plays a minor role; rather, it reflects the fact that trees at both sites are already operating near hydraulic limits because of chronic salinity and submersion stress. Under these conditions, modest increases in VPD can substantially raise the risk of hydraulic failure by accelerating sap flow and increasing xylem vulnerability to embolism. At the same time, instantaneous A_n^{et} remains relatively buffered, due to the hyperbolic relationship between stomatal conductance and photosynthesis in the Farquhar model (Farquhar & von Caemmerer, 1982) and modest biochemical stimulation from warming. Thus, elevated temperature acts as an additional stressor superimposed on a pre-stressed system, increasing mortality risk without strongly reducing carbon uptake.

4.2 Elevated CO_2 enhances carbon assimilation but not water status

Simulations under elevated CO_2 showed consistent increases in A_{net} and leaf biomass in both species (Figs. 2e–h, 4e–h), consistent with numerous field and experimental studies (Drake et al., 1997; Ainsworth & Long, 2005; Walker et al., 2020). Improved resource-use efficiency under elevated CO_2 may be especially beneficial under light- or nutrient-limited conditions typical of saturated coastal ecosystems. Trees likely responded to greater carbon availability by increasing leaf area.

However, elevated CO_2 had a minimal impact on tree hydraulic status. At the Chesapeake Bay site, the simulated soil salinity regime is characterized by a gradual, seasonally varying increase from near-fresh to low-to-moderate brackish conditions, rather than abrupt exposure to full-strength seawater. As a result, trees experience chronic but relatively moderate osmotic and ionic

stress superimposed on prolonged waterlogging. In our simulations, coastal tree mortality therefore arises primarily from impaired root function caused by long-term root loss, rather than from soil water deficits. Stomata do respond to high VPD and rising salinity, but once fine-root biomass and conductance have been strongly reduced, further reductions in gs provide limited additional hydraulic protection because water uptake is constrained by damaged roots rather than by transpiration demand (Li et al., 2022; Ding et al., 2023; Ding et al., 2025). Under these conditions, CO_2-induced reductions in transpiration are insufficient to offset mortality risk driven by chronic root loss.

4.3 Similar tree-level responses emerge from shared stress pathways

Broadleaf and conifer trees showed comparable physiological responses to elevated CO_2 and temperature (Figs. 3–4), largely because both experienced similar degrees of root loss under inundation (Ding et al., 2025). While species differ in traits such as leaf habit and architecture, environmental forcing—especially saturation and salinity—was the primary driver of mortality. Trait differences shaped the magnitude but not the direction of responses.

Some distinctions still emerged. Conifers exhibited slightly higher mortality under elevated temperature, possibly due to year-round transpiration by evergreen canopies (Fig. 3). Both species responded similarly to elevated CO_2, likely due to similar Vc_{max} parameterization. These findings suggest that environmental constraints can override interspecific trait differences.

4.4 Vegetation drives divergent ecosystem trajectories

Despite similar individual-level responses to elevated CO_2 and temperature, ecosystems diverged in their trajectories following tree mortality and marsh expansion. In broadleaf systems, tree loss created canopy openings that allowed marsh plants to establish quickly, maintaining total LAI and GPP despite climate-induced stress (Fig. 5). In contrast, conifer systems—characterized by higher initial stand density and closed canopies—experienced sharper declines in LAI and GPP, with marsh colonization too slow to fully compensate for the loss of tree cover (Fig. 6).

These contrasting outcomes reflect initial differences in vegetation structure derived from site-specific census data. The model was initialized using observed size structures at each site, which

resulted in a less dense, more open broadleaf forest at Lake Erie and a denser conifer forest at Chesapeake Bay. This structural difference shaped subsequent ecosystem dynamics. The lower canopy density and more open structure of broadleaf forests facilitated more rapid marsh invasion, enabling those systems to recover functionally even as tree mortality increased. The high water-use efficiency of marsh species, further enhanced by elevated CO_2, contributed to this compensatory response. However, in dense conifer stands mortality led to abrupt structural collapse, and the slow replacement by marsh vegetation limited ecosystem recovery. Although higher conifer mortality also eventually creates canopy openings, the key difference is the timing of gap formation relative to the pace of marsh colonization: in the broadleaf system, lower initial stand density allows mortality to create small, distributed gaps early in the simulation that are quickly colonized by marsh plants, whereas in the dense conifer system, high initial crown closure delays the formation of contiguous open patches sufficient for marsh establishment, resulting in a pronounced lag between tree loss and vegetation recovery. These contrasting responses highlight how differences in initial stand structure, canopy openness, and regenerative capacity, rather than physiology alone, determine long-term trajectories of coastal ecosystems under climate change.

4.5 Implications for modeling vegetation responses under elevated CO_2 and temperature

Most ecosystem models emphasize physiological processes such as CO_2 fertilization, but underrepresent mortality and community shifts. Our findings show that changes in vegetation composition—mediated by mortality and marsh colonization—are at least as important as, and often more influential than, physiological adjustments alone in determining ecosystem responses to elevated CO_2 and temperature in the coastal forests we studied (Figs. 7–8). This conclusion emerges despite our use of a single, moderately salt-sensitive parameter set for long-term salinity and hypoxia tolerance in both tree types. A more detailed representation of species-specific tolerance would likely modify the quantitative thresholds for mortality and marsh expansion, and could even allow some particularly tolerant species to persist longer under high salinity. However, we expect the qualitative pattern—that stand structure, canopy openness, and regenerative capacity strongly modulate how climate change reshapes coastal forest–marsh mosaics—to remain robust. Our results therefore argue for Earth system models that couple

physiological responses with explicit mortality, demographic turnover, and vegetation dynamics, including trait variation in submersion and salt tolerance.

Neglecting mortality due to hydraulic failure and subsequent vegetation reorganization may lead to overestimating the long-term benefits of CO_2 enrichment and underestimating ecosystem vulnerability. Our results support growing recognition that demographic and community-level processes are critical to understanding ecosystem feedbacks to climate change (Franklin et al., 2016; Felton & Smith, 2017).

4.6 Limitations and future study

Despite the species-based parameterization of photosynthetic, hydraulic, and allometric traits, our representation of stress tolerance is still limited by the scarcity of species-specific data on long-term responses to salinity and flooding. In particular, we lack direct constraints on salinity and hypoxia tolerance for the swamp white oak and loblolly pine stands considered here, and therefore adopted a single, moderately salt-sensitive parameter set calibrated at a coastal conifer site. This limitation implies that our quantitative projections of mortality rates for any given species should be interpreted with caution. We view the most robust aspects of our results as the relative patterns and mechanisms, for example, how differences in stand structure, phenology, and local hydrology modulate vulnerability—rather than precise predictions of species-specific thresholds under future climate and sea-level rise.

An important limitation of the present study is that we lack species-specific constraints on long-term tolerance to chronic salinity and hypoxia for the focal coastal forests. Consequently, we applied a single set of salinity and flooding tolerance parameters—calibrated at a coastal conifer site (Beaver Creek) based on Sitka spruce responses—to both the broadleaf and conifer trees at Lake Erie and Chesapeake Bay. This simplifying assumption allows us to cleanly isolate the roles of stand structure, phenology, and local hydrologic forcing in shaping future vulnerability, but it likely underestimates the true diversity of stress-tolerance strategies among coastal species. Future work should explore how interspecific variation in salinity and flooding tolerance modulates the patterns reported here.

4.7 Summary

In summary, simulations with FATES-Hydro show that elevated temperature intensifies hydraulic stress and coastal forest tree mortality, while elevated CO_2 enhances carbon assimilation without improving water status under flooding. At the ecosystem scale, marsh invasion offsets tree loss in broadleaf forests but reduces productivity in conifer systems. These responses are governed more by vegetation composition and stand structure than by physiology alone. To improve projections of future carbon and water dynamics, ecosystem models must integrate plant hydraulics, mortality, and vegetation dynamics.

Acknowledgments

JD, NM, BBL, KM, NW, JPM, PR, SCP, MW, TM, PT, and VB were supported by COMPASS-FME, a multi-institutional project supported by the U.S. Department of Energy, Office of Science, Biological and Environmental Research as part of the Environmental System Science Program. The Pacific Northwest National Laboratory is operated for DOE by Battelle Memorial Institute under contract DE-AC05-76RL01830.Any use of trade, product or firm names is for descriptive purposes only and does not imply endorsement by the U.S. Government. MK acknowledges the support of the U.S. National Science Foundation (#1654374, #1832221, #2012670).

Author contributions

JD and NM designed the study and drafted the manuscript. JD developed the model and performed simulations. CDK helped with model development. NM, NW, LS, DD, KM, MK, PR, PZ, HZ, SP, SW, WW, WI, AS, TM, PT, and JPM collected field data or performed data analysis. All the authors contributed to the manuscript.

Competing interests

None declared

Open Research

The data and FATES-Hydro code that support the findings of this study are openly available in GitHub repository: https://github.com/JunyanDing/FATES_COMPASS or Zenodo (Ding et al., 2025b): https://doi.org/10.5281/zenodo.15116449

References

Ainsworth, E. A., & Long, S. P. (2005). What have we learned from 15 years of free-air CO_2 enrichment (FACE)? A meta-analytic review of the responses of photosynthesis, canopy properties and plant production to rising CO_2. New Phytologist, 165(2), 351–372. https://doi.org/10.1111/j.1469-8137.2004.01224.x

Arkema, K. K., Guannel, G., Verutes, G., Wood, S. A., Guerry, A., Ruckelshaus, M., Kareiva, P., Lacayo, M., & Silver, J. M. (2013). Coastal habitats shield people and property from sea-level rise and storms. Nature Climate Change, 3(10), 913–918. https://doi.org/10.1038/nclimate1944

Ball, J. T., Woodrow, I. E., & Berry, J. A. (1987). A model predicting stomatal conductance and its contribution to the control of photosynthesis under different environmental conditions. In Progress in Photosynthesis Research (pp. 221–224). Springer.

Bamber, J. L., Oppenheimer, M., Kopp, R. E., Aspinall, W. P., & Cooke, R. M. (2019). Ice sheet contributions to future sea-level rise from structured expert judgment. Proceedings of the National Academy of Sciences, 116(23), 11195–11200. https://doi.org/10.1073/pnas.1817205116

Barbier, E. B. (2013). Valuing ecosystem services for coastal wetland protection and restoration: Progress and challenges. Resources, 2(3), 213–230. https://doi.org/10.3390/resources2030213

Burlakova, L. E., Karatayev, A. Y., Pennuto, C., & Mayer, C. (2014). Changes in Lake Erie benthos over the last 50 years: Historical perspectives, current status, and main drivers. Journal of Great Lakes Research, 40(3), 560–573. https://doi.org/10.1016/j.jglr.2014.05.012

Chen, J., & Kirwan, M. L. (2022). Coastal forest retreat and wetland migration in response to sea-level rise. Environmental Research Letters, 17(9), 094043. https://doi.org/10.1088/1748-9326/ac853c

Christoffersen, B. O., Gloor, M., Fauset, S., Fyllas, N. M., Galbraith, D. R., Baker, T. R., … & Malhi, Y. (2016). Linking hydraulic traits to tropical forest function in a size-structured and trait-driven model (TFS v.1-Hydro). Geoscientific Model Development, 9(11), 4227–4255.

Ding, J., Buotte, P., Bales, R., Christoffersen, B., Fisher, R. A., Goulden, M., … & Koven, C. D. (2023a). Understanding the interplay of rooting and hydraulic strategies on the response of conifer forest stands to multiyear drought in the Southern Sierra Nevada of California. Biogeosciences, 20, 4491–4510. https://doi.org/10.5194/bg-20-4491-2023

Ding, J., McDowell, N., Bailey, V., Conroy, N., Day, D. J., Fang, Y., Kemner, K. M., Kirwan, M. L., Koven, C. D., Kovach, M., … & Wilson, S. J. (2025). Modeling the mechanisms of coastal vegetation dynamics and ecosystem responses to changing water levels. Biogeosciences, 22(22), 6963–6978.

Ding, J., McDowell, N., Fang, Y., Ward, N., Kirwan, M. L., Regier, P., … & Li, W. (2023b). Modeling the mechanisms of conifer mortality under seawater exposure. New Phytologist. https://doi.org/10.1111/nph.19076

592 Drake, B. G., Gonzàlez-Meler, M. A., & Long, S. P. (1997). More efficient plants: A
593 consequence of rising atmospheric CO_2? Annual Review of Plant Physiology and Plant
594 Molecular Biology, 48, 609–639.

595 Duarte, C. M., Losada, I. J., Hendriks, I. E., Mazarrasa, I., & Marbà, N. (2013). The role of
596 coastal plant communities for climate change mitigation and adaptation. Nature Climate
597 Change, 3(11), 961–968. https://doi.org/10.1038/nclimate1970

598 Ezer, T., & Corlett, W. B. (2012). Is sea level rise accelerating in the Chesapeake Bay? A novel
599 approach for analyzing sea-level data. Geophysical Research Letters, 39(19), L19605.
600 https://doi.org/10.1029/2012GL053435

601 Falster, D. S., Duursma, R. A., Ishihara, M. I., Barneche, D. R., FitzJohn, R. G., Vårhammar, A.,
602 … & York, R. A. (2015). BAAD: a Biomass and Allometry Database for woody plants.
603 Ecology, 96(5), 1445–1445. https://doi.org/10.1890/14-1889.1

604 Farquhar, G. D., & von Caemmerer, S. (1982). Modelling of photosynthetic response to
605 environmental conditions. In Physiological Plant Ecology II (pp. 549–587). Springer.

606 FATES Development Team. (2021). FATES Technical Documentation. https://fates-users-
607 guide.readthedocs.io/projects/tech-doc/en/latest/

608 Felton, A. J., & Smith, M. D. (2017). Integrating plant ecological responses to climate extremes
609 from individual to ecosystem levels. Philosophical Transactions of the Royal Society B,
610 372(1723), 20160142. https://doi.org/10.1098/rstb.2016.0142

611 Fisher, R. A., Koven, C. D., Anderegg, W. R. L., Christoffersen, B. O., Dietze, M. C., Farrior, C.
612 E., … & Xu, C. (2015). Taking off the training wheels: The properties of a dynamic
613 vegetation model without climate envelopes. Geoscientific Model Development, 8(11),
614 3593–3619.

615 Fisher, R. A., Koven, C. D., Anderegg, W. R. L., et al. (2018). Vegetation demographics in Earth
616 System Models: A review of progress and priorities. Global Change Biology, 24(1), 35–
617 54. https://doi.org/10.1111/gcb.13910

618 Franklin, J. F., Spies, T. A., Van Pelt, R., Carey, A. B., Thornburgh, D. A., Berg, D. R., … &
619 Chen, J. (2002). Disturbances and structural development of natural forest ecosystems
620 with silvicultural implications, using Douglas-fir forests as an example. Forest Ecology
621 and Management, 155(1–3), 399–423. https://doi.org/10.1016/S0378-1127(01)00575-8

622 Gedan, K. B., Silliman, B. R., & Bertness, M. D. (2009). Centuries of human-driven change in
623 salt marsh ecosystems. Annual Review of Marine Science, 1, 117–141.
624 https://doi.org/10.1146/annurev.marine.010908.163930

Golaz, J.-C., Caldwell, P. M., Van Roekel, L. P., et al. (2019). The DOE E3SM coupled model version 1: Overview and evaluation at standard resolution. Journal of Advances in Modeling Earth Systems, 11(7), 2089–2129. https://doi.org/10.1029/2018MS001603

Grossiord, C., Buckley, T. N., Cernusak, L. A., et al. (2020). Plant responses to rising vapor pressure deficit. New Phytologist, 226(6), 1550–1566. https://doi.org/10.1111/nph.16485

Harris, I. C. (2019). CRU JRA v2.0: A forcings dataset combining CRU TS and JRA-55 [Dataset]. University of East Anglia Climatic Research Unit & Japan Meteorological Agency.

IPCC. (2021). Climate Change 2021: The Physical Science Basis. Cambridge University Press.

Kirwan, M. L., & Megonigal, J. P. (2013). Tidal wetland stability in the face of human impacts and sea-level rise. Nature, 504(7478), 53–60. https://doi.org/10.1038/nature12856

Koven, C. D., Fisher, R. A., Knox, R. G., Christoffersen, B. O., Chambers, J. Q., Dietze, M. C., … & Wieder, W. R. (2020). Benchmarking and parameter sensitivity of plant hydraulics in the E3SM land model version 1.0. Geoscientific Model Development, 13(11), 4425–4443.

Li, W., McDowell, N. G., Zhang, H., Wang, W., Mackay, D. S., Leff, R., … & Myers-Pigg, A. N. (2022). The influence of increasing atmospheric CO_2, temperature, and vapor pressure deficit on seawater-induced tree mortality. New Phytologist, 235(5), 1767–1779.

Manzoni, S., Vico, G., Katul, G., Palmroth, S., Jackson, R. B., & Porporato, A. (2013). Hydraulic limits on maximum transpiration and the emergence of the safety–efficiency trade-off. New Phytologist, 198(1), 169–178.

McDowell, N. G., Sapes, G., Pivovaroff, A., Adams, H., Allen, C. D., Anderegg, W. R. L., … & Xu, C. (2022). Mechanisms of woody plant mortality under rising drought, CO_2, and vapor pressure deficit. Nature Reviews Earth & Environment. https://doi.org/10.1038/s43017-022-00272-1

Meinshausen, M., Nicholls, Z. R. J., Lewis, J., et al. (2020). The SSP greenhouse gas concentrations and their extensions to 2100. Geoscientific Model Development, 13(8), 3571–3605. https://doi.org/10.5194/gmd-13-3571-2020

Mitsch, W. J., Bernal, B., Nahlik, A. M., Mander, Ü., Zhang, L., Anderson, C. J., Jørgensen, S. E., & Brix, H. (2015). Wetlands, carbon, and climate change. Landscape Ecology, 30(1), 1–20. https://doi.org/10.1007/s10980-014-0151-4

Munns, R., & Tester, M. (2008). Mechanisms of salinity tolerance. Annual Review of Plant Biology, 59, 651–681. https://doi.org/10.1146/annurev.arplant.59.032607.092911

658 NOAA STAR. (2023). Sea Level Rise and Coastal Flooding Impacts Viewer.
659 https://www.star.nesdis.noaa.gov/socd/lsa/SeaLevelRise/

660 NOAA. (2023). Sea Level Trends. National Oceanic and Atmospheric Administration.
661 https://tidesandcurrents.noaa.gov/sltrends/

662 Oleson, K. W., Lawrence, D. M., Bonan, G. B., Drewniak, B., Huang, M., Koven, C. D., … &
663 Yang, Z. (2013). Technical description of version 4.5 of the Community Land Model
664 (CLM). NCAR Technical Note NCAR/TN-503+STR.

665 Perri, S., Katul, G. G., & Molini, A. (2019). Xylem–phloem hydraulic coupling explains multiple
666 osmoregulatory responses to salt stress. New Phytologist, 224, 644–662.
667 https://doi.org/10.1111/nph.15812

668 Perri, S., Viola, F., Noto, L. V., & Molini, A. (2017). Salinity and periodic inundation controls
669 on the soil–plant–atmosphere continuum of gray mangroves. Hydrological Processes, 31,
670 1271–1282. https://doi.org/10.1002/hyp.11109

671 Robbins, Z. J., Chambers, J. Q., Christoffersen, B. O., Fisher, R. A., Knox, R. G., Koven, C. D.,
672 … & McDowell, N. G. (2024). Future climate doubles the risk of hydraulic failure in a
673 wet tropical forest. New Phytologist, 244(6), 2239–2250.

674 Sallenger, A. H., Doran, K. S., & Howd, P. A. (2012). Hotspot of accelerated sea-level rise on
675 the Atlantic coast of North America. Nature Climate Change, 2(12), 884–888.

676 Schieder, N. W., Walters, D. C., & Kirwan, M. L. (2018). Massive upland to wetland conversion
677 compensated for historical marsh loss in Chesapeake Bay, USA. Estuaries and Coasts,
678 41(4), 940–951.

679 Sippo, J. Z., Lovelock, C. E., Santos, I. R., Sanders, C. J., & Maher, D. T. (2018). Mangrove
680 mortality in a changing climate: An overview. Estuarine, Coastal and Shelf Science, 215,
681 241–249. https://doi.org/10.1016/j.ecss.2018.10.011

682 Smith, I. M., & Kirwan, M. L. (2021). Salinity control on the ecological function of tidal
683 marshes in Chesapeake Bay. Limnology and Oceanography Letters, 6(6), 429–436.

684 Spalding, M. D., Ruffo, S., Lacambra, C., Meliane, I., Hale, L. Z., Shepard, C. C., & Beck, M.
685 W. (2014). The role of ecosystems in coastal protection: Adapting to climate change and
686 coastal hazards. Ocean & Coastal Management, 90, 50–57.
687 https://doi.org/10.1016/j.ocecoaman.2013.09.007

688 Tagestad, J. D., Ustin, S. L., Rejmánková, E., & Tuxen, K. A. (2021). Remote sensing of
689 wetland vegetation dynamics. Remote Sensing of Environment, 256, 112316.
690 https://doi.org/10.1016/j.rse.2021.112316

691 Walker, A. P., De Kauwe, M. G., Bastos, A., Belmecheri, S., Georgiou, K., Keeling, R., … &
692 Norby, R. J. (2020). Integrating the evidence for a terrestrial carbon sink caused by
693 increasing atmospheric CO_2. New Phytologist, 229(5), 2413–2445.
694 https://doi.org/10.1111/nph.16866

695 Way, D. A., & Montgomery, R. A. (2015). Photoperiod constraints on tree phenology,
696 performance and migration in a warming world. Plant, Cell & Environment, 38(9), 1725–
697 1736. https://doi.org/10.1111/pce.12431

698 Xu, C., Christoffersen, B., Robbins, Z., Knox, R., Fisher, R. A., Chitra-Tarak, R., Slot, M.,
699 Kueppers, L., Trotochaud, J., Powell, T. L., & McDowell, N. G. (2023). Quantification of
700 hydraulic trait control on plant hydrodynamics and risk of hydraulic failure within a
701 demographic structured vegetation model in a tropical forest (FATES-HYDRO V1.0).
702 Geoscientific Model Development, 16(21), 6267–6283. https://doi.org/10.5194/gmd-16-
703 6267-2023

704 Zeng, X. (2001). Global vegetation root distribution for land modeling. Journal of
705 Hydrometeorology, 2(5), 525–530.

706 Zhang, P., McDowell, N. G., Zhou, X., Wang, W., Leff, R. T., Pivovaroff, A. L., Zhang, H.,
707 Chow, P. S., Ward, N. D., Indivero, J., & Yabusaki, S. B. (2021). Declining carbohydrate
708 content of Sitka-spruce trees dying from seawater exposure. Plant Physiology, 185,
709 1682–1696. https://doi.org/10.1093/plphys/kiab002

710 Ding, J., McDowell, N., Bailey, V., Conroy, N., Day, D. J., Fang, Y., Kemner, K. M., Kirwan,
711 M. L., Koven, C. D., Kovach, M., & Wilson, S. J. (2025b). FATES-COMPASS model
712 code and data for coastal vegetation dynamics simulations [Software/Data]. Zenodo.
713 https://doi.org/10.5281/zenodo.15116449

714

Figure captions

Fig. 1. Effects of elevated CO_2 and temperature on broadleaf tree physiology, expressed as treatment minus control. Panels show (a, b) loss of xylem hydraulic conductivity (K/K_{max}), (c, d) mortality rate, (e, f) net leaf carbon assimilation rate (A_{net}), and (g, h) total leaf biomass per tree. Results are shown for both Chesapeake Bay and Lake Erie sites.

Fig. 2. Effects of elevated CO_2 and temperature on conifer tree physiology, expressed as treatment minus control. Panels show (a, b) loss of xylem hydraulic conductivity, (c, d) mortality rate, (e, f) net leaf carbon assimilation rate (A_{net}), and (g, h) total leaf biomass per tree at both sites.

Fig. 3. Comparison of hydraulic responses and mortality between each treatment and the control for broadleaf and conifer trees. Each point represents the annual mean value for one simulation year at one site. The x-axis shows values under the historical climate (Control), and the y-axis shows the corresponding values under the elevated CO_2 (HCO2), elevated temperature (HT), or combined (HCO2&HT) treatments. Panels show scatterplots of xylem conductance for (a, c) broadleaf and (b, d) conifer trees, and mortality rate for (e, g) broadleaf and (f, h) conifer trees. The 1:1 line indicates no treatment effect; points above the line indicate higher values under the treatment than under the control, and points below the line indicate lower values.

Fig. 4. Comparison of leaf-level carbon responses between each treatment and the control. Each point represents the annual mean value for one simulation year at one site. The x-axis shows values under the historical climate (Control), and the y-axis shows the corresponding values under the elevated CO_2 (HCO2), elevated temperature (HT), or combined (HCO2&HT) treatments. Panels show scatterplots of net leaf carbon assimilation (Anet) for (a, c) broadleaf and (b, d) conifer trees, and total leaf biomass for (e, g) broadleaf and (f, h) conifer trees. The 1:1 line indicates no treatment effect; points above the line indicate higher values under the treatment than under the control, and points below the line indicate lower values.

Fig. 5. Ecosystem responses of broadleaf forest under elevated CO_2 and temperature. Panels show changes in (a, b) leaf area index (LAI), (c, d) gross primary productivity (GPP), and (e, f) transpiration at the Chesapeake Bay and Lake Erie sites.

Fig. 6. Ecosystem responses of conifer forest under elevated CO_2 and temperature. Panels show changes in (a, b) leaf area index (LAI), (c, d) gross primary productivity (GPP), and (e, f) transpiration at the two sites.

Fig. 7. Relationship between vegetation composition and ecosystem function in broadleaf forests. Panels show standardized gross primary productivity (GPP; a, b) and transpiration (E_t; c, d) as a function of the marsh-to-tree abundance ratio under different climate scenarios.

Fig. 8. Relationship between vegetation composition and ecosystem function in conifer forests. Panels show standardized gross primary productivity (GPP; a, b) and transpiration (E_t; c, d) as a function of the marsh-to-tree abundance ratio across scenarios.

753

754 Fig. 1

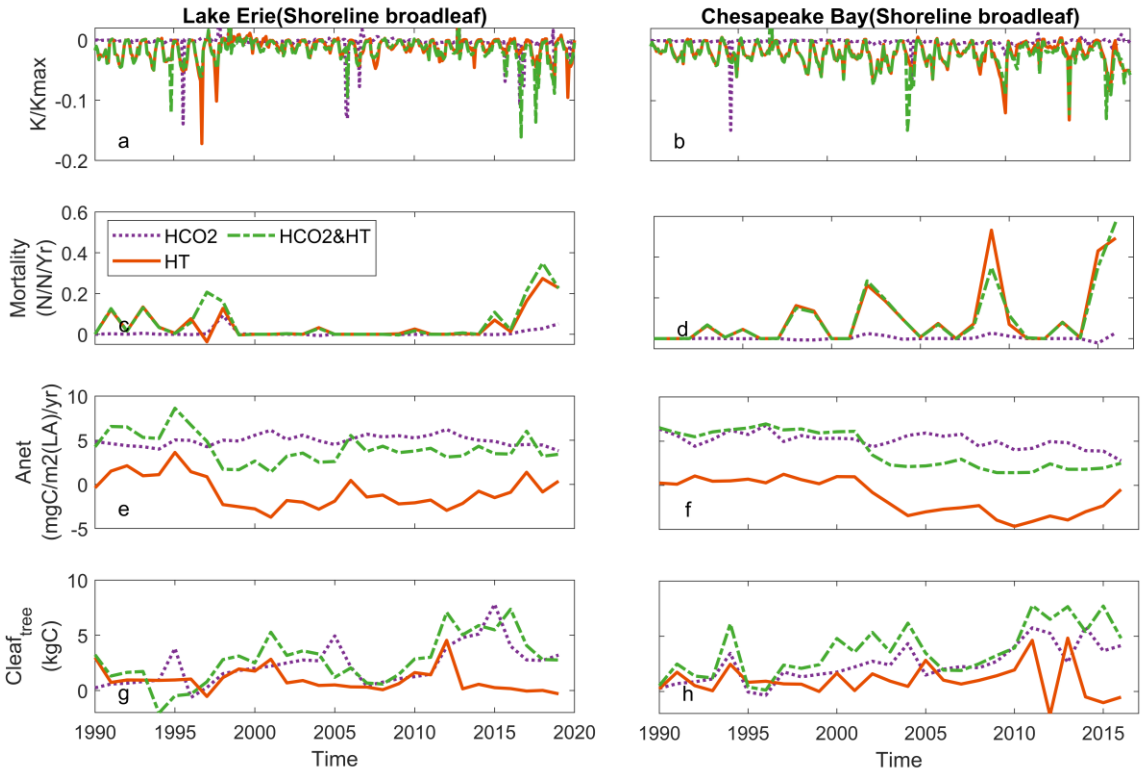

755

756

757 Fig. 2

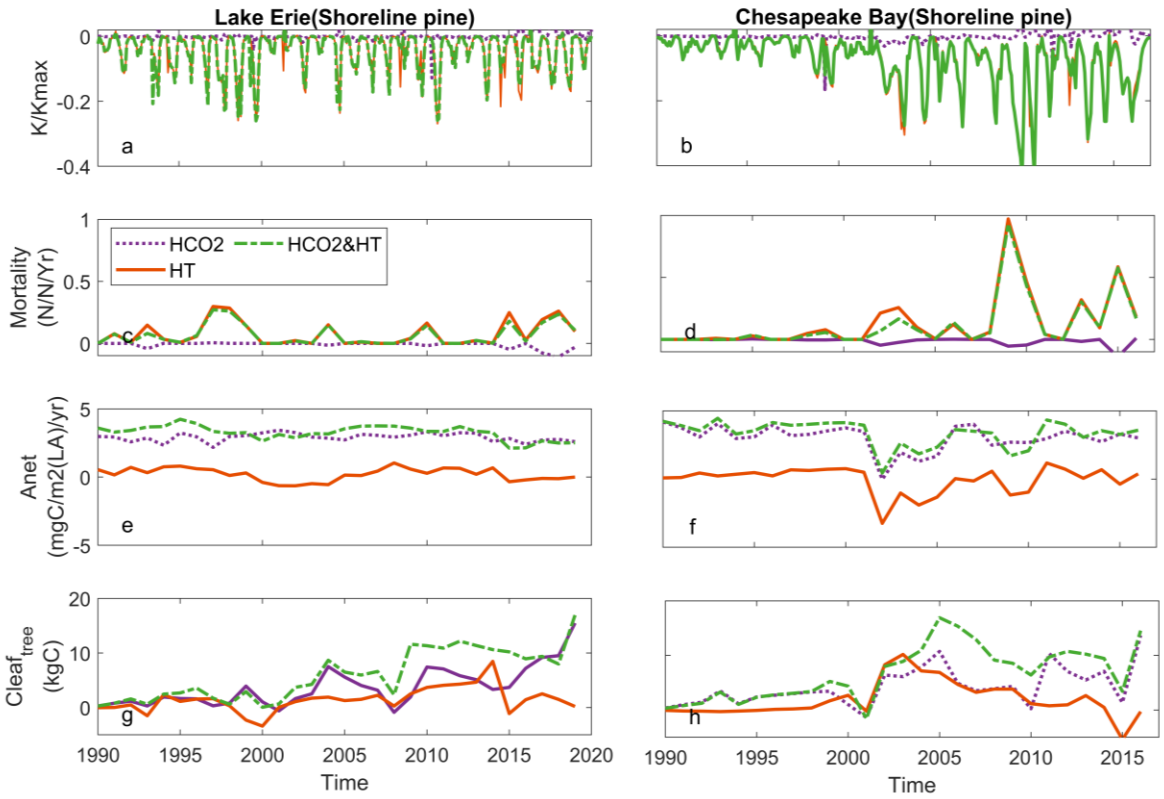

758

759

760 Fig. 3

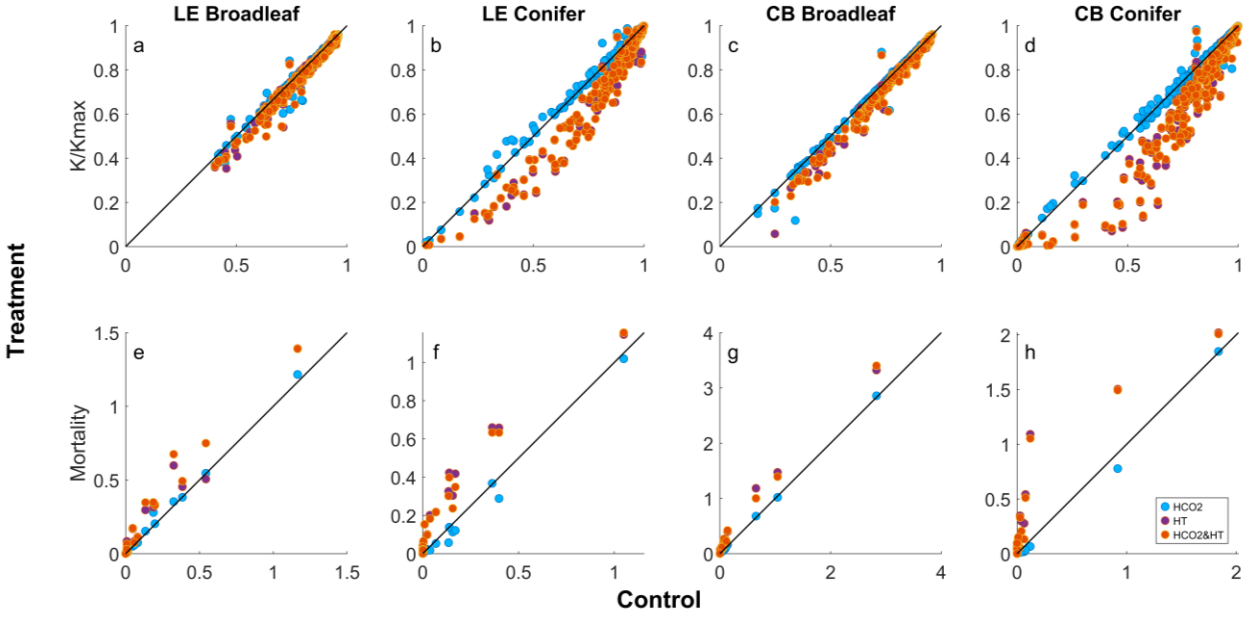

761

762

763 Fig. 4

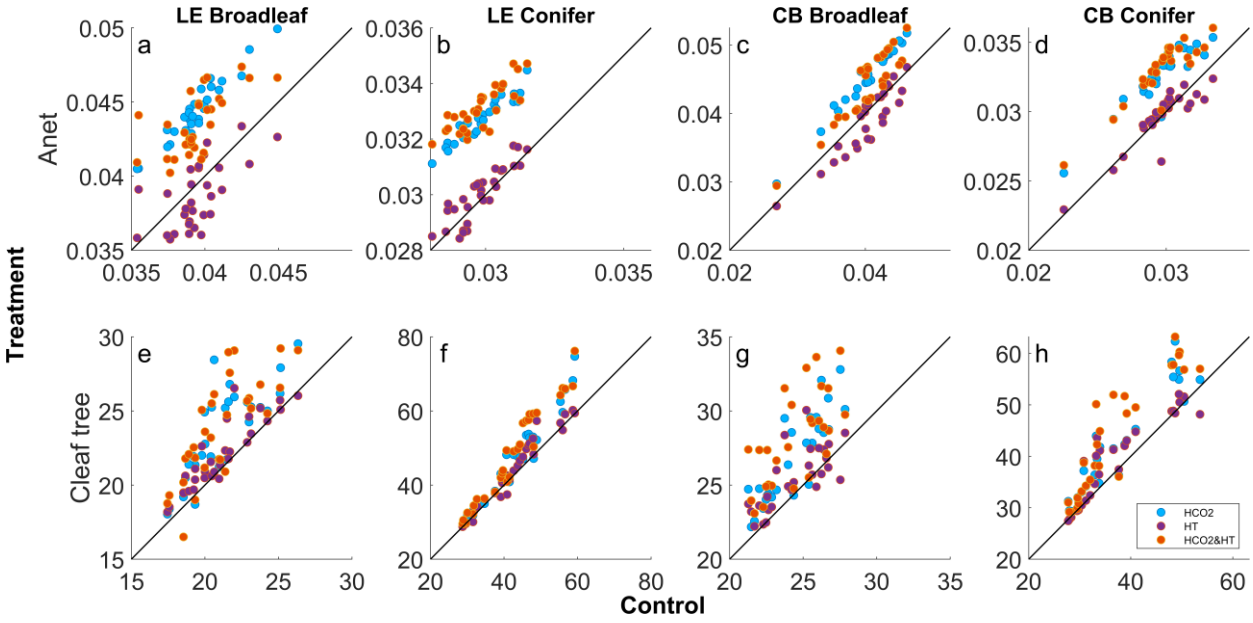

764

765

766 Fig. 5

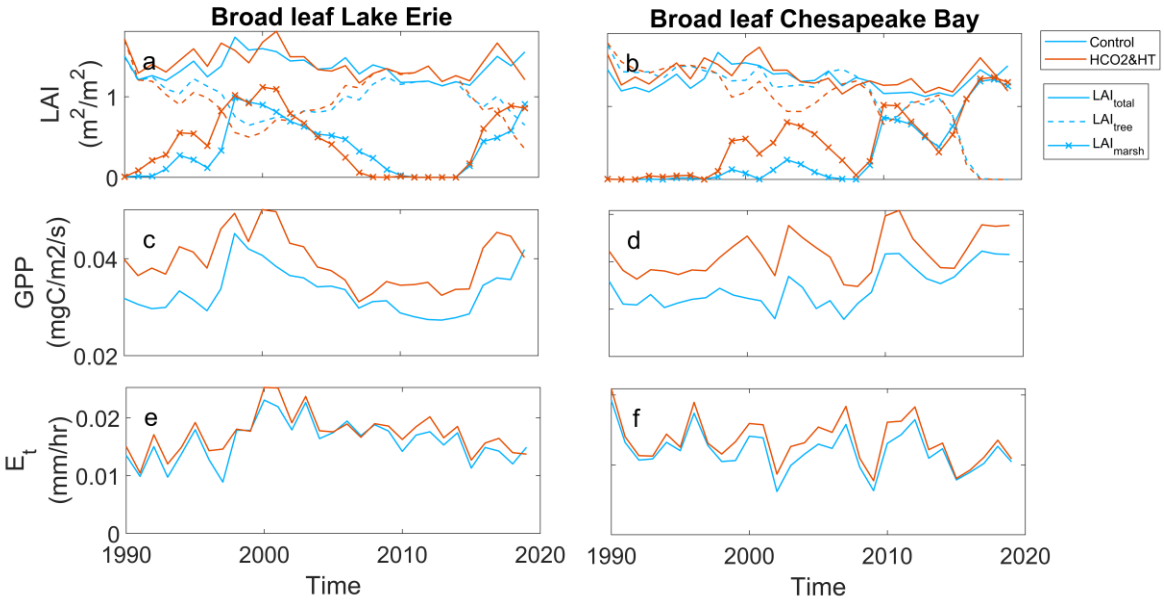

767

768

769 Fig. 6

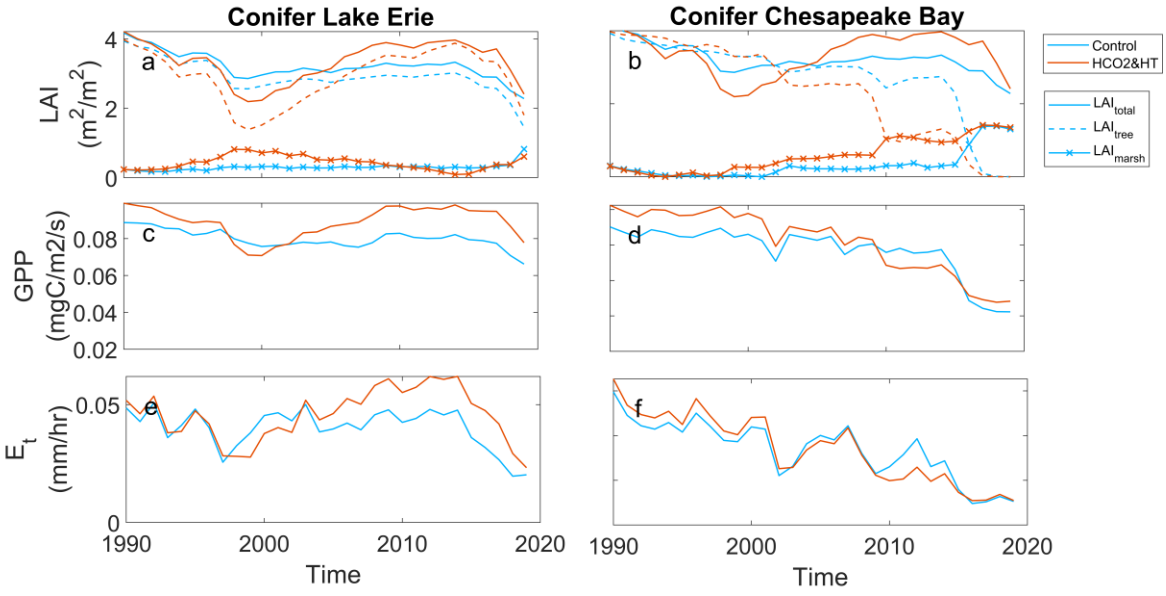

770

771

772 Fig. 7

773

774

775 Fig. 8

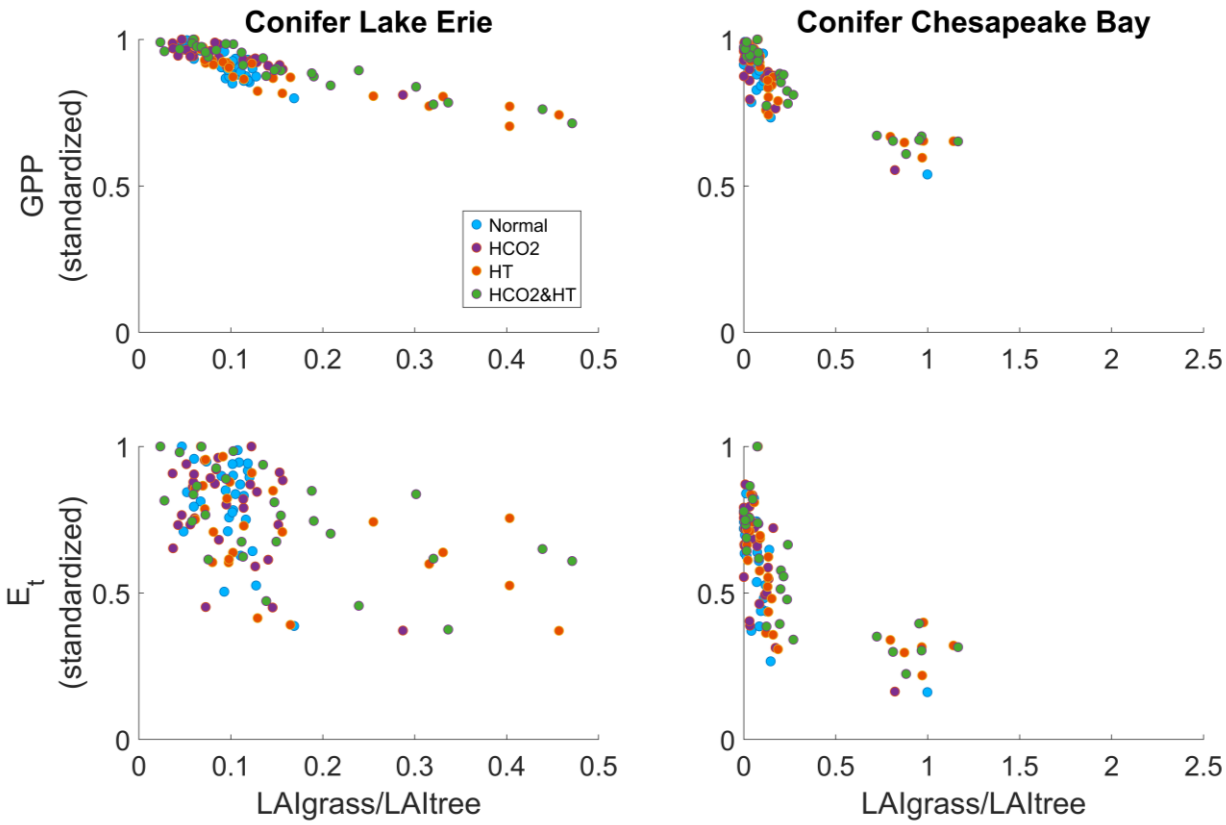
Conifer Lake Erie
Conifer Chesapeake Bay
GPP (standardized)
E_t (standardized)
LAIgrass/LAItree
LAIgrass/LAItree
Normal
HCO2
HT
HCO2&HT
0
0.5
1
0.1
0.2
0.3
0.4
1.5
2
2.5

776